NASA TECHNICAL NOTE

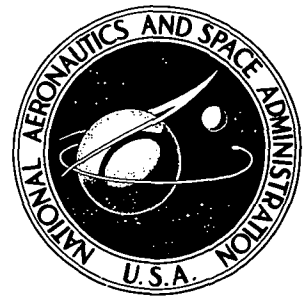

NASA TN D-7222

NASA TN D-7222

EXPERIMENTAL AND ANALYTICAL DETERMINATION OF STABILITY PARAMETERS FOR A BALLOON TETHERED IN A WIND

by L. Tracy Redd, Robert M. Bennett, and Samuel R. Bland

Langley Research Center
Hampton, Va. 23665

NATIONAL AERONAUTICS AND SPACE ADMINISTRATION • WASHINGTON, D. C. • SEPTEMBER 1973

1. Report No. NASA TN D-7222	2. Government Accession No.	3. Recipient's Catalog No.
4. Title and Subtitle EXPERIMENTAL AND ANALYTICAL DETERMINATION OF STABILITY PARAMETERS FOR A BALLOON TETHERED IN A WIND		5. Report Date September 1973 6. Performing Organization Code
7. Author(s) L. Tracy Redd, Robert M. Bennett, and Samuel R. Bland		8. Performing Organization Report No. L-8524 10. Work Unit No. 501-22-04-01
9. Performing Organization Name and Address NASA Langley Research Center Hampton, Va. 23665		11. Contract or Grant No. 13. Type of Report and Period Covered Technical Note
12. Sponsoring Agency Name and Address National Aeronautics and Space Administration Washington, D.C. 20546		14. Sponsoring Agency Code

15. Supplementary Notes

16. Abstract

Experimental and analytical techniques for determining stability parameters for a balloon tethered in a steady wind are described. These techniques are applied to a particular 7.64-meter-long balloon, and the results are presented. The stability parameters of interest appear as coefficients in linearized stability equations and are derived from the various forces and moments acting on the balloon. In several cases the results from the experimental and analytical techniques are compared and suggestions are given as to which techniques are the most practical means of determining values for the stability parameters.

17. Key Words (Suggested by Author(s))	18. Distribution Statement
Aerostat Stability parameters Tethered balloons	Unclassified – Unlimited

19. Security Classif. (of this report)	20. Security Classif. (of this page)	21. No. of Pages	22. Price*
Unclassified	Unclassified	57	$3.00

*For sale by the National Technical Information Service, Springfield, Virginia 22151

CONTENTS

EXPERIMENTAL AND ANALYTICAL DETERMINATION OF STABILITY PARAMETERS FOR A BALLOON TETHERED IN A WIND

By L. Tracy Redd, Robert M. Bennett, and Samuel R. Bland
Langley Research Center

SUMMARY

Experimental and analytical techniques for determining stability parameters for a balloon tethered in a steady wind are described. These techniques are applied to a particular 7.64-meter-long balloon, and the results are presented. The stability parameters of interest appear as coefficients in linearized stability equations and are derived from the various forces and moments acting on the balloon. In several cases the results from the experimental and analytical techniques are compared and suggestions are given as to which techniques are the most practical means of determining values for the stability parameters.

INTRODUCTION

A tethered balloon is useful for a number of purposes, such as supporting antennas or providing an aerial platform. Such operations are often impaired by the occurrence of dynamic instabilities, especially during strong wind conditions. Although information relating to the stability of towed and tethered bodies, including balloons, has been published (see, e.g., refs. 1 to 4), a systematic procedure for the analysis of the stability of tethered balloons is needed. In an attempt to fill this need, the Langley Research Center undertook a general research study to develop improved techniques for predicting the stability of tethered balloons.

Portions of the Langley study are given in references 5 to 8. Reference 5 describes the preliminary version of the towing technique that was developed and used to measure aerodynamic forces on inflated balloons. Reference 6 presents the derivation of the stability equations, a comparison of analytical with experimental results, and a stability-parameter trend study. Reference 7 contains a listing and description of the computer programs used for calculating and plotting the analytical results. A brief overview of the complete study is given in reference 8.

The purpose of this paper is to describe methods of obtaining values for the stability parameters required for the analysis of the stability of a tethered balloon. These

methods are illustrated by their application to a particular 7.64-meter balloon used in the Langley stability studies. When possible, the analytically determined values of the parameters are compared with their measured values.

SYMBOLS

A perpendicular distance from balloon axis of symmetry to a support cable as used in the roll-inertia test, m (see fig. 6)

a distance along balloon center line from nose to structural center of mass, m (see fig. 2)

B buoyancy force, N

b distance along balloon center line from nose to center of buoyancy, m (see fig. 2)

b_1, b_2, b_3 distances parallel to balloon center line from structural center of mass of balloon to front-cable attachment, rear-cable attachment, and center of buoyancy, respectively, m (see fig. 10)

C_D drag coefficient, $\left.\frac{D}{\rho V^2 S/2}\right|_t$

C_L lift coefficient, $\left.\frac{L}{\rho V^2 S/2}\right|_t$

$C_{L,T}$ lift coefficient for the tail fins, $\left.\frac{L_T}{\rho V^2 S/2}\right|_t$

$\left(C_{L_\alpha}\right)_T = \frac{\partial C_{L,T}}{\partial \alpha}$

C_l rolling-moment coefficient, $\left.\frac{M_X}{\rho V^2 S \bar{c}/2}\right|_t$

C_m pitching-moment coefficient, $\left.\frac{M_Y}{\rho V^2 S \bar{c}/2}\right|_t$

$C_{m,T}$ pitching-moment coefficient for tail fins, $\left.\frac{M_{Y,T}}{\rho V^2 S \bar{c}/2}\right|_t$

$\left(C_{m_\alpha}\right)_T = \frac{\partial C_{m,T}}{\partial \alpha}$

C_n	yawing-moment coefficient, $\left.\frac{M_Z}{\rho V^2 S\bar{c}/2}\right\|_t$
C_Y	side-force coefficient, $\left.\frac{F_Y}{\rho V^2 S/2}\right\|_t$
c	distance along balloon center line from nose to effective center of aerodynamic apparent mass, m (see fig. 2)
c_1, c_2	distances from balloon center of mass to front- and rear-cable attachment points, respectively, for yaw-inertia test, m (see fig. 8)
$\bar{c}$	balloon length, m
D	aerodynamic drag force, N
e_1	distance from balloon center of mass to elastic axis (e.a.), m (see fig. 8(b))
F_1, F_2, F_3, F_4	tensions in front and rear restraining cables used in aerostatic tests, N (see figs. 3 and 4)
F_B	negative buoyancy force of inflation air for aerostatic tests, N
F_Y	force along the Y-axis, N
g	acceleration of gravity, m/sec^2
h	perpendicular distance from center line of balloon to load-band plane, m (see fig. 10)
h_j	width of hull segment, m
h_T	perpendicular distance from balloon center line to aerodynamic center of tail fin for planform A, m (see fig. 11)
I_Q	mass moment of inertia of compound-pendulum system about knife-edge support, $kg\text{-}m^2$

I_{xx}, I_{yy}, I_{zz} total moments of inertia about balloon center of mass, in the X'',Y'',Z'' axis system (including aerodynamic apparent inertias), kg-m^2 (see fig. 2 for axis system)

$I_{xx,a}, I_{yy,a}, I_{zz,a}$ moments of inertia of aerodynamic apparent mass about its own centroid, kg-m^2

$I_{xx,f}$ roll inertia of trifilar-pendulum support frame, kg-m^2

$I_{xx,g}, I_{yy,g}, I_{zz,g}$ moments of inertia of inflation gas about its own center of mass, kg-m^2

$I_{xx,s}, I_{yy,s}, I_{zz,s}$ moments of inertia of balloon structure about its own center of mass, kg-m^2

$I_{zz,f}$ yaw inertia of the compound-pendulum support frame, kg-m^2 (see fig. 7)

$I_{zz,Q}$ combined yawing moment of inertia of the balloon structure, inflation gas, and apparent mass about knife-edge support, kg-m^2 (see figs. 7 and 13)

$$K = m_w g l_Q - B(l_Q - b) + m_s g(l_Q - a) + m_f g l_f$$

k_1 apparent-mass coefficient (see eq. (8))

$$k_{yy} = \frac{T_1 + T_2}{l_1}$$

$$k_{\psi\psi} = \frac{T_1 l_F^2 + T_2 l_R^2}{l_1}$$

L aerodynamic lift force, N

L_T aerodynamic lift force due to tail-fin assembly, N

l_1 length of tether cables used in bifilar-pendulum tests, m (see figs. 5 and 8)

l_2 length of support cables used in roll-inertia test, m (see fig. 6)

l_e distance from balloon nose to elastic axis (e.a.), m (see fig. 8)

l_F distance from elastic axis (e.a.) to front tether cable for yaw-inertia test, m (see fig. 8)

l_{FC} distance from balloon nose to front tether cable as used in the yaw-inertia test, m (see fig. 8)

l_f distance from knife-edge support to center of gravity of support frame, m (see fig. 7)

l_Q distance from knife-edge support to nose of balloon, m (see fig. 7)

l_R distance from elastic axis (e.a.) to rear tether cable for yaw-inertia test, m (see fig. 8)

l_S length of support frame for compound-pendulum test, m (see fig. 7)

l_T distance parallel to balloon center line from reference point to aerodynamic center of tail-fin assembly, m (see fig. 11)

l_{TH} distance between front and rear cables for yaw-inertia test, m (see fig. 8)

l_x distance along balloon center line from nose to center of mass of balloon (including aerodynamic apparent mass), m (see fig. 2)

$\overline{M}$ mean molecular weight of a gas, kg/mole

M_X, M_Y, M_Z aerodynamic rolling, pitching, and yawing moments about the X-, Y-, and Z-axes, respectively, N-m

$M_{Y,T}$ aerodynamic pitching moment due to tail-fin assembly, N-m

m_f mass of support frame used in compound-pendulum test, kg (see fig. 7)

m_g mass of inflation gas, kg

m_s mass of balloon structure without bridle or payload, $\frac{W_s}{g}$, kg

m_w	mass of ballast added to balloon nose for compound-pendulum test, kg (see fig. 7)
$m_{x,a}, m_{y,a}, m_{z,a}$	aerodynamic apparent mass associated with balloon acceleration along X''-, Y''-, and Z''-axes, respectively, kg (see fig. 2 for axis system)
$m_{x,t}, m_{y,t}, m_{z,t}$	total mass of balloon for accelerations along X''-, Y''-, and Z''-axes, respectively, for $\alpha_t = 0$, kg
P	oscillation period, sec/cycle
$\tilde{p}$	absolute pressure, N/m^2
p,q,r	rolling, pitching, and yawing rates about X-, Y-, and Z-axes, respectively, rad/sec
R^*	universal gas constant, J/K-mole
$\bar{R}$	engineering gas constant, $\frac{R^*}{\bar{M}}$, J/K-kg
S	reference area of balloon, $V_b^{2/3}$, m^2
T	sum of tensions in trifilar-pendulum cables, N (see eq. (11) and fig. 6)
T_1, T_2, T_3, T_4	tensions in front and rear tether cables, N (see figs. 5, 8, and 10)
T^*	absolute temperature, kelvins
V	steady wind velocity, m/sec
V_b	volume of balloon hull, m^3
W_s	structural weight of balloon without bridle or payload, N
X,Y,Z	stability axis system; for steady-state conditions, X-axis is parallel to steady horizontal wind vector (see fig. 10 for axis system)
X'', Y'', Z''	body-fixed axis system; X''-axis is along balloon axis of symmetry (see fig. 2 for axis system)

x,y,z	displacements along X-, Y-, and Z-axes, m
x'',y'',z''	displacements along X''-, Y''-, and Z''-axes, m
x_j	distance from balloon nose to center of mass of a hull segment, m
x_n	distance from elastic axis (e.a.) to node line, m (see fig. 8)
y_1,y_2	lateral displacements of upper ends of front and rear cables, respectively, for yaw-inertia test, m (see fig. 8(b))
y_3	lateral displacement of elastic axis (e.a.) in yaw-inertia test, m (see fig. 8(b))
α	perturbation angle of attack of X-axis, $\dot{z}/V + \theta$, rad
α_t	trim angle of attack, rad or deg
α_{lb}	angle of attack of tow-truck load bar, rad (see fig. 10)
α_p	effective angle of attack of tail-fin assembly due to rolling rate p, rad
β	angle of sideslip, rad
θ,ϕ,ψ	angles of pitch, roll, and yaw, respectively, rad
ρ	atmospheric density, kg/m^3
ρ_g	density of inflation gas at standard atmospheric conditions, kg/m^3
φ	angular displacement of balloon tether lines in XZ-plane for bifilar-pendulum test, rad (see fig. 5)
$\varphi_1,\varphi_2,\varphi_3,\varphi_4$	angular displacements of balloon tow lines in XZ-plane, rad (see fig. 10)
ω	frequency, rad/sec

Subscripts:

air	inflation gas is air
e	ambient air outside the balloon hull
g	balloon inflation gas
He	inflation gas is helium
t	balloon at trim condition
vac	vacuum conditions

Subscripts used with the aerodynamic coefficients denote derivatives as follows:

α	with respect to α
$\dot{\alpha}$	with respect to $\frac{\dot{\alpha}\bar{c}}{2V}$
β	with respect to β
$\dot{\beta}$	with respect to $\frac{\dot{\beta}\bar{c}}{2V}$
p	with respect to $\frac{p\bar{c}}{2V}$
q	with respect to $\frac{q\bar{c}}{2V}$
r	with respect to $\frac{r\bar{c}}{2V}$

Dots over a symbol indicate derivatives with respect to time.

GENERAL COMMENTS

In the present study four types of parameters were required for the analysis of the stability of a tethered balloon:

(1) Aerostatic properties (e.g., weight and buoyancy)

(2) Masses and moments of inertia (including apparent mass)

(3) Aerodynamic coefficients and derivatives

(4) Tether-cable properties

These parameters appear as coefficients in the linearized stability equations of reference 6 and are typical of those needed in other studies of the stability of towed or tethered bodies (refs. 1 to 4 and 9 and 10, e.g.). The values of these parameters, with the exception of the tether-cable properties, were determined by techniques described in the subsequent sections of this paper. The tether-cable properties are not discussed in this paper since some of these properties were measured directly and the rest were determined analytically by methods of reference 6.

To obtain the values of the required balloon stability parameters, it was necessary to develop both analytical and experimental methods. The aerostatic properties were determined experimentally. The masses and moments of inertia were determined both analytically and experimentally, and the results were compared. The static aerodynamic lift, drag, and pitching-moment coefficients were determined experimentally from tow tests, and the remainder of the aerodynamic stability parameters were derived analytically.

The 7.64-meter-long balloon used in the Langley stability study is shown in figure 1, and its geometrical properties are given in table I and figure 2.

The balloon geometry shown in table I was obtained by combining the forward portion of a C-class airship configuration (ref. 11) of fineness ratio 2 with a conical aft section to provide an overall fineness ratio of 3. The conical aft section joined the C-class portion at the point where the slopes were tangent. The nose of the balloon was also slightly more spherical than that of the regular C-class airship configuration.

The essential components of the balloon were a hull (i.e., gas bag) constructed of nylon and saran, and a tail-fin assembly. A load band was attached to the lower portion of the hull to permit variations in the bridle attachment points and, hence, make it possible to change the balloon trim angle of attack. The tail assembly consisted of four fins, each with a balsa spar framework covered with aluminized Mylar sheeting. The fins were connected together by rings at their front and rear and by a number of small cables that could be adjusted to aline the fins with the balloon center line. The tail assembly was connected to attachment patches on the hull at four points for each fin. The balloon was designed to operate with a constant pressure differential; therefore, a relief valve was provided to avoid overinflation.

DESCRIPTION OF ANALYTICAL AND EXPERIMENTAL TECHNIQUES

The balloon used in the present study was axially symmetric (fig. 1) except for the load band. Therefore, the effect of the load band was neglected and the masses, moments of inertia, and aerodynamic forces associated with motions in the z''-direction (fig. 2) were assumed to be the same as those for motions in the y''-direction. The values of the stability parameters thus obtained were for the axially symmetric balloon and did not include the effect of the bridle or payload. The effects of the bridle and payload (e.g., test instruments) were later added to the results of the present report to obtain the properties of the fully instrumented balloon as used for the study of reference 6.

AEROSTATIC PROPERTIES

The required aerostatic quantities a, b, B, m_g, V_b, and W_s were determined experimentally from several tests. The basic structural weight W_s was found by weighing the deflated balloon. The remaining parameters were determined from two different tests with the inflated balloon constrained by two cables. In the first test (fig. 3) the balloon was inflated with helium; in the second test (fig. 4), with air. The first test was used to determine the buoyancy B from the measured tensions F_1 and F_2 by the equation

$$B = F_1 + F_2 + W_s \tag{1}$$

The volume V_b and mass of the inflation gas m_g for the balloon were then computed by use of the perfect gas law (ref. 12) to give

$$V_b = \frac{B}{\left(1 - \frac{\tilde{p}_g}{\tilde{p}_e}\frac{\bar{R}_e}{\bar{R}_g}\right)\frac{g\tilde{p}_e}{\bar{R}_e T^*}} \tag{2}$$

$$m_g = \rho_g V_b \tag{3}$$

where e refers to the external ambient air and g refers to the inflation gas. The volume can also be calculated from the balloon geometry.

The locations of the structural center of mass a and of the center of buoyancy b are obtained by summing the moments about the nose for the two tests (figs. 3 and 4) to give

$$aW_s - bB = -\bar{c}F_2 \tag{4}$$

and

$$aW_S + bF_B = \bar{c}F_4 \tag{5}$$

The negative buoyancy F_B of the inflation air in the second test was too small to measure with the test instrumentation; therefore, it was computed from the perfect gas law as follows:

$$F_B = \frac{gV_b\left(\tilde{p}_g - \tilde{p}_e\right)}{\bar{R}_e T^*}$$

Solution of equations (4) and (5) yields

$$a = \frac{\bar{c}\left(BF_4 - F_B F_2\right)}{W_S\left(B + F_B\right)} \tag{6}$$

$$b = \frac{\bar{c}\left(F_2 + F_4\right)}{B + F_B} \tag{7}$$

MASSES AND MOMENTS OF INERTIA

In the present study both analytical and experimental methods were used to obtain the mass and inertial properties of the balloon. Some of the experimental methods were considered to be impractical for use with balloons larger than the 7.64-meter balloon. Therefore, analytical methods which could be used with larger balloons without difficulty were also developed. The validity of the analytical methods was evaluated by comparing the analytical results with those measured experimentally.

Analytical Estimates

The analytical techniques were applied by considering the balloon system to be composed of three parts: the inflation gas, the balloon structure, and the apparent air mass associated with the balloon accelerations. The mass and inertia of each of these parts were determined separately and then summed in an appropriate manner to obtain the mass and inertia of the entire balloon.

Inflation gas.- The mass and inertial properties of the inflation gas were calculated by assuming the inflated balloon hull to be divided into 35 segments. These segments were formed by analytically slicing the hull normal to its axis of symmetry, as shown in sketch 1. The gas in each segment was assumed to be rigid and to form a frustum of a

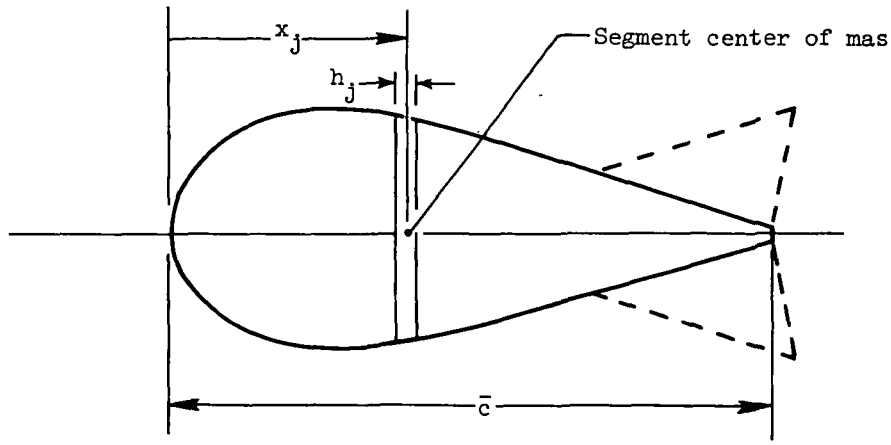

Sketch 1

right circular solid cone. The volume, mass, centroid location, and inertias about all three axes at the segment center of mass were calculated for each gas segment. The results were transferred from the segment centers of mass to the center of mass of the inflation gas and numerically integrated to obtain the total mass and inertial properties of the gas.

Balloon structure.- The theoretical mass and inertial properties of the balloon structure were obtained by assuming the balloon to consist of two components: a hull and a tail-fin assembly. The properties of the total structure were obtained by appropriately combining the properties of these two components.

The hull mass and inertial properties were obtained by assuming the hull skin to be a rigid shell with a shape the same as that of the fully inflated balloon. The shell mass was assumed to be uniformly distributed (except for the seam tapes) and equal to the mass of the fabric of the balloon hull. The shell was divided into 35 segmental rings in the shape of truncated hollow cones, of the same widths h_j as those used in calculating the mass of the inflation gas. The seam tape elements attached to each segment were assumed to be point masses appropriately distributed among the segments. The mass, inertias, and centroid location of each segment were calculated and the results were transferred to the shell center of mass. These results were then summed to give the mass and inertial properties for the total balloon hull.

The mass and inertial properties of the tail-fin assembly were calculated by transferring the mass and inertias of each tail fin and fin ring (fig. 1) to the assembly center of mass and summing the results. Similarly, the mass and inertias of each tail fin were determined by transferring the mass and inertias of each balsa spar and Mylar sheet to the fin center of mass and summing the results.

Apparent air mass.- When a body immersed in a fluid is accelerating, a certain amount of the surrounding fluid moves with the body. That portion of the fluid set in motion is referred to as the aerodynamic apparent mass, or simply apparent mass. Because the mass of the fluid (i.e., air) involved in the present study is of the same order of magnitude as the combined masses of the balloon structure and lifting gas, the apparent mass must be considered as part of the mass of the balloon system.

The apparent mass of air associated with an elongated body accelerating parallel to its axis of symmetry is different from that for motions perpendicular to the axis of symmetry (ref. 13). Although the magnitudes of these masses are different, it is assumed in the present study that their respective mass centroids are all located on the axis of symmetry. Also, because of axial symmetry, it is assumed that the centroids are located at the same distance c (fig. 2) aft of the balloon nose for motions in both the y''- and z''-directions.

The value of the apparent mass for acceleration along the X''-axis $m_{x,a}$ was calculated by methods given in reference 13. In using these methods it was assumed that the aft end of the balloon hull came to a point and that the apparent mass associated with the tail fins for motions along the X''-axis was negligible. Furthermore, $m_{x,a}$ was assumed to be proportional to V_b and ρ; thus,

$$m_{x,a} = k_1 \rho V_b \tag{8}$$

where k_1 is the apparent-mass coefficient which varies according to the width-length ratio of the hull $(k_1 = 0.220$ for the present analysis$)$.

The terms for the apparent masses and inertias, other than $m_{x,a}$, were calculated from procedures given in reference 14. In using these procedures, the balloon was divided into two sections, as shown in sketch 2, where section ①, or balloon "fuselage" section, includes all the hull forward of the roots of the tail-fin leading edges; and section ②, or balloon "tail fin" section, includes the tail fins and the portion of the hull aft of the root of the tail-fin leading edges.

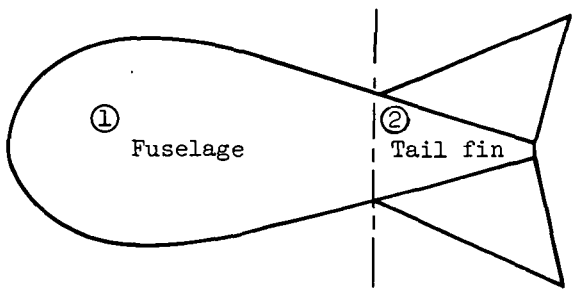

Sketch 2

The equations for determining the apparent masses and inertias of the fuselage and tail-fin sections are given in detail in reference 14 and, therefore, are not presented in this report. In using these equations, it should be remembered that since the balloon is axially symmetric, $m_{z,a}$ and $I_{zz,a}$ are equal to $m_{y,a}$ and $I_{yy,a}$, respectively. The apparent roll inertia of the fuselage section is also assumed to be negligible when compared with that of the tail section.

Experimental Measurements

Four different types of test were required to measure the mass and inertial properties. The first test was used to obtain the apparent mass for motion along the X"-axis (fig. 2), the second was needed to measure the roll inertia, and the remaining two were used to determine the yaw inertia and mass associated with motions along the Y"-axis. Because the balloon was considered to be axially symmetric, the pitch inertia and mass associated with vertical motions along the Z"-axis were assumed to be equal, respectively, to the yaw inertia and mass associated with lateral motions.

Longitudinal apparent mass $m_{x,a}$.- In order to determine experimentally the value of $m_{x,a}$, the balloon can be inflated with helium and tethered by two parallel cables to form an inverted bifilar-pendulum system, as shown in figure 5. If the longitudinal angle of oscillation φ of the parallel cables is small and the damping is neglected, the forces can be summed in the x-direction to give the equation of motion for the pendulum system:

$$m_{x,t}\ddot{x} + (T_1 + T_2)\frac{x}{l_1} = 0$$

Since the period of oscillation P is

$$P = 2\pi\sqrt{\frac{l_1 m_{x,t}}{T_1 + T_2}}$$

and

$$m_{x,t} = m_s + m_{x,a} + m_g$$

then

$$m_{x,a} = \frac{T_1 + T_2}{4\pi^2 l_1} P^2 - (m_s + m_g) \tag{9}$$

Since T_1, T_2, and P are measured during the oscillation tests, and l_1, m_s, and m_g can be measured directly or by methods described in the section "Aerostatic Properties,"

then $m_{x,a}$ can be obtained directly from equation (9). (Note, eq. (9) can be ill conditioned if $m_{x,a} << m_s + m_g$.)

Roll inertia.- In order to determine the roll inertia of a balloon, it can be suspended in a vacuum test chamber by three flexible cables of equal lengths and distances from the axis of symmetry to form a trifilar pendulum, as shown in figure 6. Assuming that the damping is negligible and the rolling oscillations are small, the equation of motion about the pendulum center line is

$$I_{xx}\ddot{\phi} + T\frac{A^2}{l_2}\phi = 0$$

The roll inertia I_{xx} can be expressed in terms of the period of oscillation P and also in terms of its component parts as follows:

$$I_{xx} = \frac{T}{l_2}\left(\frac{AP}{2\pi}\right)^2 = I_{xx,a} + I_{xx,f} + I_{xx,g} + I_{xx,s} \tag{10}$$

The expression for the sum of the cable tensions T is found from the total weight and buoyancy of the pendulum system and is as follows:

$$T = m_s g + m_f g - B \tag{11}$$

If the oscillation tests are performed in a vacuum, then $I_{xx,a}$ and $I_{xx,g}$ are negligible and the roll inertia of the balloon structure $I_{xx,s}$ can be determined directly from equation (10), provided the roll inertia of the support frame is also known. Furthermore, by subtracting the value of the roll inertia $I_{xx,vac}$ measured in a vacuum from the roll inertia I_{xx} obtained at atmospheric pressure, the sum of the roll inertias of the apparent mass and the inflation gas can be obtained from equation (10) as follows:

$$\Delta I_{xx} = I_{xx} - I_{xx,vac} = \frac{A^2}{4\pi^2 l_2}\left[TP^2 - (TP^2)_{vac}\right] = I_{xx,a} + I_{xx,g} \tag{12}$$

The combined values of $I_{xx,a}$ and $I_{xx,g}$ in equation (12) can be separated by testing the balloon at the same atmospheric pressure but with different inflation gases, for example, air and helium. An additional relationship derived from the perfect gas law (ref. 12) must also be used with equation (12). This relationship is

$$(I_{xx,g})_{air} = (I_{xx,g})_{He}\left[\frac{(\bar{R}T^*)_{He}}{(\bar{R}T^*)_{air}}\right]_{\tilde{p}_e=\text{Const},\,\tilde{p}_g=\text{Const}} \tag{13}$$

where the subscripts air and He designate air and helium inflation gases.

Yaw inertia and other mass properties.- The yawing moments of inertia I_{zz}, $I_{zz,s}$, $I_{zz,g}$, and $I_{zz,a}$ and the mass properties $m_{y,t}$, $m_{y,a}$, c, and l_x can be determined by the two pendulum tests shown in figures 7 and 8. For the first test (fig. 7) the balloon is suspended from a knife-edge support so that the balloon swings as a compound pendulum. For the second test (fig. 8) the balloon is inflated with helium and tethered by two cables to form a bifilar pendulum which has two degrees of freedom – yaw ψ and side translation y.

The compound-pendulum test (fig. 7) is a common experimental method for determining the masses and moments of inertia of a body. (See, ref. 15, e.g.) In applying this method to the present case, special care must be taken to insure that the balloon retains its fully inflated shape during the tests. A ballast weight is also needed in some instances to provide sufficient restoring force to overcome the buoyancy of the inflation gas.

The equation of motion for the compound-pendulum system used in the present study (fig. 7) is obtained by summing moments of inertia about the knife-edge support. If the damping is assumed negligible and the yaw angles ψ are small, this equation is

$$I_Q\ddot{\psi} + K\psi = 0 \tag{14}$$

where

$$K = m_w g l_Q - B(l_Q - b) + m_s g(l_Q - a) + m_f g l_f$$

Thus the expression for I_Q in terms of its period of oscillation P is

$$I_Q = \frac{KP^2}{4\pi^2} \tag{15}$$

The inertia I_Q of the pendulum system can be expressed in terms of the masses and inertias of its component parts by use of the parallel-axis theorem to give

$$I_Q = I_{zz,s} + m_s(l_Q - a)^2 + I_{zz,f} + m_f l_f^2 + I_{zz,g} + m_g(l_Q - b)^2 + I_{zz,a} + m_{y,a}(l_Q - c)^2 + m_w l_Q^2 \tag{16}$$

where the moment of inertia of the ballast about its own center of gravity is assumed to be negligible.

If the balloon is tested in a vacuum, then the inflation-gas and apparent-mass terms in equation (16) become negligibly small. Thus, for these conditions the inertia of the

balloon structure $I_{yy,s}$ can be determined from equation (15) and the remaining expressions in equation (16), provided the mass and inertia of the support frame and ballast weight are known. The mass and inertia of the support frame can, of course, be determined by oscillating the frame without the balloon. By subtracting the inertia $I_{Q,vac}$ obtained in a vacuum from the inertia I_Q measured at atmospheric conditions, the inertias of the apparent mass and the inflation gas are obtained as follows:

$$\Delta I_Q = I_Q - I_{Q,vac} = \left[KP^2 - (KP^2)_{vac}\right]\frac{1}{4\pi^2} \tag{17}$$

where

$$\Delta I_Q = I_{zz,g} + m_g(l_Q - b)^2 + I_{zz,a} + m_{y,a}(l_Q - c)^2 \tag{18}$$

The equations of motion for the bifilar-pendulum system (figs. 8(a) and (b)) are derived in the appendix. The working forms of these equations are

$$m_{y,t}\left(1 - \frac{l_x - l_e}{x_n}\right) = \frac{k_{yy}}{\omega^2} \tag{19}$$

$$I_{zz} - (l_x - l_e)x_n\frac{k_{yy}}{\omega^2} = \frac{k_{\psi\psi}}{\omega^2} \tag{20}$$

where

$$m_{y,t} = m_s + m_g + m_{y,a} \tag{21}$$

$$I_{zz} = I_{zz,s} + m_s(a - l_x)^2 + I_{zz,g} + m_g(l_x - b)^2 + I_{zz,a} + m_{y,a}(l_x - c)^2 \tag{22}$$

$$l_x = \frac{m_s a + m_g b + m_{y,a} c}{m_s + m_g + m_{y,a}} \tag{23}$$

and ω is the oscillation frequency of the system.

Equations (18) to (23) provide a set of six equations with seven unknowns, namely, I_{zz}, $I_{zz,a}$, $I_{zz,g}$, $m_{y,t}$, $m_{y,a}$, l_x, and c. All other terms in these equations can be obtained from direct measurements or by tests described in the section entitled "Aerostatic Properties" and in the appendix.

Since the preceding equations contain one too many unknowns, it is suggested that the analytical value of $I_{yy,g}$ be used because this term is the most straightforward to calculate. Thus, equations (18) to (23) can be solved simultaneously to find the six remaining unknowns.

AERODYNAMIC COEFFICIENTS AND DERIVATIVES

Lift, Drag, and Pitching-Moment Coefficients

The aerodynamic forces on an inflated balloon are generally obtained from wind-tunnel tests of a rigid model (refs. 16 and 17, e.g.). Such test methods do not account for deformations of the flexible balloon structure, which may be significant at certain load conditions. For this reason, a tow-test technique was developed to measure the static aerodynamic forces and moments acting on a flexible inflated balloon at various angles of attack and wind speeds.

The basic difference between the tow-test technique and conventional wind-tunnel methods is that the forces and moments on the balloon are measured from the tensions in the tow cables rather than on conventional force balances. Thus, the towed balloon does not have to be rigidly mounted and can have structural deformations and some freedom of motion.

Description of test technique.- The tow-test technique used in this study is illustrated in figures 9 and 10. In figure 9, the balloon is shown attached to a panel truck by two cables and a load bar. The panel truck provides space for instrumentation and acts as a towing vehicle. The load bar is attached to the truck by means of a pivot so that its angle of attack can be varied. The load bar is also equipped with load cells to measure the cable tensions and with potentiometers to measure the cable angles with respect to the load bar. The speed of the truck relative to the air and the sideslip angle are measured by an anemometer (i.e., wind sensor) mounted at the front of the truck. Outputs from these instruments are recorded on strip charts. Motions of the balloon are also recorded by two cameras mounted on the truck.

Determination of aerodynamic coefficients.- When the system (fig. 10) is in equilibrium, the aerodynamic forces and pitching moment L, D, and M_Y on the balloon are balanced by the balloon weight W_S, buoyancy B, and cable tensions T_3 and T_4. For this condition, the expressions for the lift, drag, and pitching moment about the reference point (figs. 2 and 10) are

$$L = W_S - B + T_3 \cos \varphi_3 + T_4 \cos \varphi_4 \tag{24}$$

$$D = T_3 \sin \varphi_3 + T_4 \sin \varphi_4 \tag{25}$$

$$M_Y = -b_3 B \cos \alpha_t + T_3\left[b_1 \cos(\varphi_3 - \alpha_t) - h \sin(\varphi_3 - \alpha_t)\right] + T_4\left[b_2 \cos(\varphi_4 - \alpha_t) - h \sin(\varphi_4 - \alpha_t)\right] \tag{26}$$

The quantities W_s, b_1, b_2, b_3, and h in these equations are determined either from direct measurements or from the aerostatic tests described previously. The quantities α_t, T_3, T_4, φ_3, and φ_4 can also be measured directly in some instances, but for the present configuration it is more convenient to calculate these quantities from the measured values of α_{lb}, T_1, T_2, φ_1, and φ_2 (fig. 10) at the lower ends of the cables. Thus for this configuration, the additional steps which are explained in the next few paragraphs are required to obtain the lift, drag, and pitching moment of the balloon.

At zero wind speed, the balloon, load bar, and tow cables form a parallelogram, so that the balloon is at the same angle of attack as the load bar and the cables are vertical. With the truck moving, the drag of the balloon causes it to ride behind its former position, so that the cables are no longer vertical. In this position, the drag on the cables and their weight act to bow the cables. In addition, if the tensions in the two cables are unequal, they will bow by different amounts, so that the balloon is no longer parallel to the load bar, as shown in sketch 3.

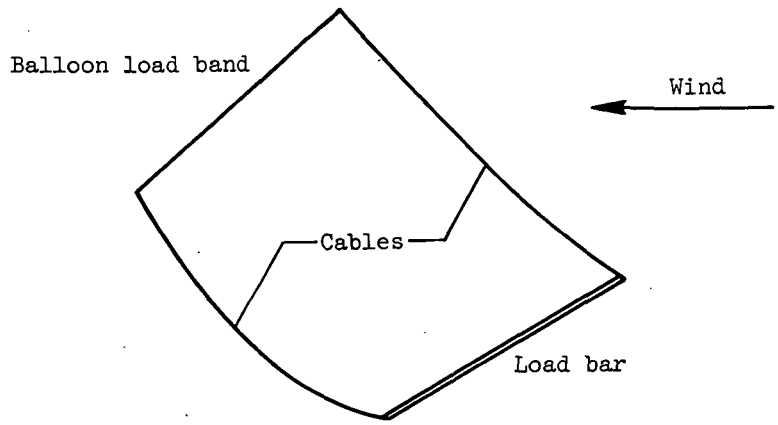

Sketch 3

To relate the tension and angles at the upper ends of the cables to those measured at the lower ends, the analysis described in appendix B of reference 6 is used. This analysis yields the position, tension, and angle of the upper end of a cable in terms of the cable length, weight, diameter, drag coefficient, wind speed, and the tension and angle at the lower end of the cable. For the present application, this is done for each cable independently; at first the constraint that the upper ends of the two cables are actually a known, fixed distance apart is ignored. This constraint is then taken into account by adjusting the measured angles at the lower ends of the cables by a small amount and repeating the cycle. This process would not have to be repeated if the cable analysis (ref. 6) gave exact results and if the cable angles φ_1 and φ_2 and tensions T_1 and T_2 could be measured precisely. Since this is not the case in the present study,

it is desirable to repeat the process in an iterative fashion until the predicted distance between the upper ends of the cables agrees with the known value.

Equations for the lift, drag, and pitching-moment coefficients can be obtained by plotting C_L, C_D, and C_m as a function of α_t and fitting least-squares curves through the resulting data points. These equations can be differentiated with respect to α_t to obtain expressions for C_{L_α}, C_{D_α}, and C_{m_α}.

Calculation of Longitudinal Dynamic Stability Derivatives

The stability derivatives C_{L_q}, C_{m_q}, $C_{L_{\dot{\alpha}}}$, and $C_{m_{\dot{\alpha}}}$ are needed in the stability analysis (ref. 6) in addition to the longitudinal static coefficients that were measured. In the present study these dynamic derivatives are determined analytically for use in the stability analysis.

Hull contributions.- The contributions of the balloon hull to the dynamic derivatives could not be analytically determined. The difficulty was that the static aerodynamic data measured for the hull with and without tail fins were insufficient to use nonslender body theory (e.g., ref. 18) for calculating these contributions. The values of C_{L_q} and C_{m_q} were obtained by using slender-body theory (e.g., refs. 18 and 19) and were found to be small compared with the tail-fin contributions. On the basis of these slender-body results and in the absence of further data, the hull contributions for the present configuration were neglected, even though the hull is not a slender body in the usual sense.

Tail-fin contributions.- Both static and rate stability derivatives were calculated for an isolated, planar tail fin by applying linear, oscillatory, lifting-surface theory to downwash deformation modes of camber, pitch, and plunge, and deriving the stability derivatives from the resulting generalized aerodynamic forces in the manner discussed, for example, in reference 20. The numerical method used, which was written and programed by Robert N. Desmarais of Langley Research Center, is an unpublished development of the method described in reference 21. On each semispan, 36 collocation points were used in the calculations.

One question that arises in the calculation of the tail-fin contributions is the treatment of the effective planform for the low-aspect-ratio surfaces attached to the relatively large, conical aft portion of the present balloon. Because of the uncertainties involved, three alternate ways of treating the effective planform were considered in the present study, as illustrated in figure 11. For planform A, the conical portion of the balloon is treated as a reflection plane and the free stream is considered to be parallel to the conical portion; for planform B, the conical aft portion of the body is included rearward from the intersection of the leading edge of the fins with the body; and for planform C, the

leading edges of the fins are projected to the center line of the body. Of the three planforms evaluated, planform A is considered to be the most realistic. The reasons for this conclusion are given in the section entitled "Dynamic Stability Derivatives."

Estimates of Lateral Stability Derivatives

None of the lateral stability derivatives were measured; hence, all these derivatives had to be estimated by other means. As was pointed out earlier, the balloon configuration was assumed to be axially symmetric. Thus, for small values of α the following lateral derivatives are assumed to correspond to the longitudinal derivatives for $\alpha_t = 0$:

$$C_{Y_\beta} = -C_{L_\alpha}\Big|_{\alpha_t=0}$$

$$C_{n_\beta} = -C_{m_\alpha}\Big|_{\alpha_t=0}$$

$$C_{Y_{\dot\beta}} = -C_{L_{\dot\alpha}}\Big|_{\alpha_t=0}$$

$$C_{n_{\dot\beta}} = -C_{m_{\dot\alpha}}\Big|_{\alpha_t=0}$$

$$C_{Y_r} = C_{L_q}\Big|_{\alpha_t=0}$$

$$C_{n_r} = C_{m_q}\Big|_{\alpha_t=0}$$

Note that the lateral derivatives are based on the length of the balloon $\bar{c}$, not the span.

Since the balloon is assumed axially symmetric, the lateral aerodynamic center is assumed to be on the center line. Thus, when $\alpha_t = 0$, the rolling moments due to sideslip β and yawing motions r are zero $\left(\text{i.e., } C_{l_\beta} = C_{l_{\dot\beta}} = C_{l_r} = 0 \text{ for } \alpha_t = 0\right)$. It is also assumed that $C_{l_{\dot\beta}} = 0$ for small values of α.

If it is assumed that the lateral aerodynamic center of the balloon remains on the center line but displaces with angle of attack as the trim angle changes from zero, then C_{l_β} becomes

$$C_{l_\beta} = C_{n_\beta} \sin \alpha_t = -C_{m_\alpha} \sin \alpha_t$$

The derivative C_{l_r} for α_t different from zero can be approximated by neglecting the aerodynamic forces on the hull. For this case the Y-force due to yawing velocity is assumed to act on the balloon center line at the position of the static aerodynamic center of the tail-fin assembly, a distance l_T (fig. 11) aft of the reference point, and displaced below the X stability axis by an amount equal to $l_T \sin \alpha_t$. Thus C_{l_r} becomes

$$C_{l_r} = -C_{Y_r} \frac{l_T}{\bar{c}} \sin \alpha_t$$

The effective angle of attack α_p of the tail-fin assembly due to rolling rate p is (ref. 22)

$$\alpha_p = \frac{p}{V} l_T \sin \alpha_t$$

Thus, if the hull effects are neglected, then the side-force and yawing-moment coefficients due to rolling motions are

$$C_Y = \left(C_{L_\alpha}\right)_T \alpha_p$$

$$C_n = -C_Y \frac{l_T}{\bar{c}} \cos \alpha_t$$

where $\left(C_{L_\alpha}\right)_T$ is the lift-curve slope calculated for the planform A tail-fin assembly. Hence, the derivatives of C_Y and C_n with respect to p are

$$C_{Y_p} = \frac{\partial C_Y}{\partial\left(\frac{p\bar{c}}{2V}\right)} = 2\left(C_{L_\alpha}\right)_T \frac{l_T}{\bar{c}} \sin \alpha_t$$

$$C_{n_p} = \frac{\partial C_n}{\partial\left(\frac{p\bar{c}}{2V}\right)} = -\left(C_{L_\alpha}\right)_T \left(\frac{l_T}{\bar{c}}\right)^2 \sin 2\alpha_t$$

The damping-in-roll derivative C_{l_p} was calculated in a similar fashion to that for the longitudinal derivatives. For planforms B and C the derivative C_{l_p} was derived directly from rolling about the center line of the balloon at $\alpha_t = 0$. For planform A the rolling about the root chord was treated and the resulting rolling moment transferred to the center line of the balloon.

It is recognized that these estimates of the lateral derivatives are simplified and may be somewhat crude. For example, estimates of C_{n_p} for airplane-type configurations involve yawing moments generated by the change in induced drag due to rolling velocity (ref. 22), which have been omitted here. Further detailed treatment was considered unwarranted, however, because of the absence of body-fin interaction data.

TEST PROCEDURES AND DISCUSSION OF RESULTS

AEROSTATIC PROPERTIES

The measured aerostatic properties defined by equations (1) to (7) and illustrated in figures 3 and 4 are shown in table II. Each of the aerostatic tests was performed at least three times and the data were averaged to obtain the results shown in the table. The scatter in the data was less than 1 percent except for V_b and B, which varied as much as 1.3 and 2.4 percent, respectively. Most of this scatter in the latter two parameters is attributed to changes in the temperature of the ambient air.

MASSES AND MOMENTS OF INERTIA

The results of the mass and inertia tests are shown in table III. This table gives the calculated and measured values of the masses and inertias of the balloon and its component parts. Since some of the experimental data are believed to be in error, the table also includes a third column, "Best estimate," which combines both experimental and calculated data to obtain the most reasonable values of the actual balloon masses and inertias. The values of the terms $m_{y,t}$, $m_{z,t}$, I_{yy}, and I_{zz} in the "Best estimate" column are each obtained by combining several balloon properties, some analytically determined and some experimentally determined. Thus, the best-estimate values for these terms are different from either their analytical or experimental values. The particular combination of balloon properties used to obtain the best-estimate values of these terms will be presented later in this section.

All the data shown in table III are for the axially symmetric balloon inflated with helium and surrounded by air at standard atmospheric conditions.

Longitudinal Apparent Mass

The experimental and calculated values of the apparent mass associated with longitudinal motion $m_{x,a}$ are given in table III. The exact agreement between these two values is believed to be a coincidence since the measured value could only be determined

to an accuracy of about 3 percent and the apparent mass of the tail fins was neglected for the calculated value.

The quantities T_1, T_2, and P in equation (9) were measured with load links and potentiometers located at the base of the tether cables (fig. 5). The tests were repeated three times and the results were averaged to obtain the value of $m_{x,a}$ shown in table III.

Roll Inertia

The trifilar-pendulum test (fig. 6) used to obtain the roll inertia of the 7.64-meter balloon was conducted in the 20-meter-diameter vacuum sphere at the Langley Research Center at air densities ranging from 0.012 to 1.29 kg/m^3. The periods of the roll oscillations were measured with a rate gyro and recorded on a strip recorder.

The combined roll inertias of the balloon structure, inflation gas, and apparent mass are plotted as a function of the vacuum-chamber density in figure 12. This figure shows that for the air-inflated balloon, the inertia of the apparent mass and inflation gas is a linear function of the test-chamber density. Test points at chamber densities other than at vacuum and atmospheric conditions were obtained for this case so that a best-fit straight line could be drawn through the points to minimize the effect of scatter in the data. This procedure gave more accurate values for I_{xx} at vacuum and atmospheric conditions.

The helium-inflated balloon was tested at chamber densities of 0.012 and 1.26 kg/m^3. For the higher density, the balloon was tethered from the vacuum-chamber floor instead of the ceiling (fig. 6) because the buoyancy force provided the restoring moment. For the lower density, the balloon was suspended from the ceiling and the structural and frame weights provided the restoring moment. There were no tests for chamber densities between these two points because the combination of buoyancy, structural weight, and frame weight did not provide sufficient restoring moments for good oscillatory motions. Although data were available for only the two chamber densities, it was assumed that the inertia of the apparent mass and inflation gas for the helium-inflated balloon was a linear function of chamber density. Thus, a best-fit straight line was also drawn through these data to minimize scatter.

The values of the roll inertias obtained from the vacuum-sphere tests and from the analysis are given in table III. This table shows that the analytical and measured values of $I_{xx,s}$ are in good agreement, but that the experimental values of $I_{xx,g}$ and $I_{xx,a}$ are considerably smaller than those calculated. The calculated value of $I_{xx,g}$ is believed to be quite accurate when all the inflation gas rotates with the hull. For the present case, however, it appears that only the portion of the gas near the hull skin rotates with the balloon. Therefore, it is believed that the measured value of $I_{xx,g}$ is

the more realistic. The measured value of $I_{xx,a}$ is also believed to be more accurate than the calculated value since the roll-inertia test is a straightforward test and some empirical estimates (ref. 14) were required to obtain the calculated value.

Yaw Inertias and Other Mass Properties

The desired yaw inertias and mass properties I_{zz}, $I_{zz,s}$, $I_{zz,a}$, $m_{y,a}$, c, and l_x for the 7.64-meter balloon were very difficult to determine experimentally because these properties were found to be functions of small differences between large values. Thus, in order to improve the prospects of obtaining accurate experimental values with the present approach, four different tests were performed with the compound-pendulum system (fig. 7). Different support lengths l_s were used for three of the tests and the fourth test used a different inflation gas. The results from each of these tests were independently combined with the results from the bifilar test (fig. 8) to give four separate values for each of the desired mass properties. These values for each property were then averaged to obtain the final experimental results listed in table III.

To increase the accuracy of the compound-pendulum test results further, enough data points were obtained to plot the yawing moment of inertia as a function of chamber density for each of the four tests. Since the yaw inertia was assumed to be a linear function of density (ref. 15), a best-fit straight line was drawn through the points for each test to minimize the effect of scatter in the data. Other approaches similar to those of reference 15 were attempted in order to obtain the desired mass properties, but the results were much worse than those obtained with the present method.

The compound-pendulum tests were conducted in the 20-meter-diameter vacuum sphere at the Langley Research Center. The test-chamber air densities ranged from 0.0016 to 1.26 kg/m^3. The three different support-frame lengths l_s used were 3.17, 6.24, and 9.24 meters, and the inflation gases were air and helium. A ballast of 4.48 kg was attached to the nose of the balloon in order to maintain a sufficient restoring force when the balloon was filled with helium. The periods of oscillation for the compound-pendulum tests were measured with an accelerometer and recorded on a strip-chart recorder.

The results of the compound-pendulum tests are shown in figure 13. The data presented are for the combined inertias of the balloon structure, inflation gas, and apparent air mass about the knife-edge support (fig. 7) as a function of vacuum-chamber density. As can be seen from figure 13, the inertias of the apparent mass and inflation gases are proportional to the chamber density, as expected. Each data point shown represents the average of three or more compound-pendulum test results. The scatter at each of these data points is less than 1 percent; hence, individual test results are not shown in the figure.

The helium inflation gas was used only for the longest support frame length l_S (fig. 13) in order to economize on time during the compound-pendulum tests. Furthermore, the helium-inflated balloon configuration could not be tested in vacuum-chamber densities greater than 0.608 kg/m^3 because of the large buoyancy force at the higher densities. Additional ballast could have been used, but this would have deformed the nose appreciably.

Some of the experimental values shown in table III are considerably different from the corresponding calculated values. The cause of these differences is attributed to scatter in the experimental data. Although the data for $I_{zz,Q}$ (fig. 13) have less than 1 percent scatter, this small amount of error combined with the errors from the bifilar-pendulum tests caused large errors (greater than 80 percent in some cases) in the experimentally determined values of I_{zz}, $I_{zz,s}$, $I_{zz,a}$, $m_{y,t}$, c, and l_x. The major problem was that the support-frame lengths l_S were too long and thus caused the terms in equations (16), (18), and (22), such as $m_s(l_Q - a)^2$, $m_g(l_Q - b)^2$, I_Q, and ΔI_Q, to be much larger than $I_{zz,s}$ or $I_{zz,a}$. Hence, a small error in a, b, l_Q, m_s, m_g, ΔI_Q, or I_Q resulted in large errors in I_{zz}, $I_{zz,s}$, and $I_{zz,a}$. As a consequence, the values of $m_{y,a}$, c, and l_x were also somewhat questionable.

Because of the uncertainty in the experimental results, the analytical values of $I_{zz,s}$, $I_{zz,a}$, $m_{y,a}$, c, and l_x were believed to be more accurate. For the same reason, the best-estimate values for I_{zz} and $m_{y,t}$ were not obtained from the experimental data but from equations (21) and (22) by combining the appropriate quantities from the "Best estimate" column of table III.

AERODYNAMIC COEFFICIENTS AND DERIVATIVES

Lift, Drag, and Pitching-Moment Coefficients

The tow tests to determine the aerodynamic lift, drag, and pitching-moment coefficients of the 7.64-meter balloon (figs. 9 and 10) were performed on a runway taxi strip at the Langley Research Center. The balloon was towed during periods of calm air, at constant speeds of from 3 to 15 m/sec (corresponding to Reynolds numbers based on $\bar{c}$ of from about 1.5×10^6 to 7.5×10^6) for an angle-of-attack range from 0^o to 24^o.

A typical strip-chart record of the tow-test measurements is shown in figure 14. As is evident in this figure, some of the data showed appreciable oscillations; hence, it was necessary to fair through the data to obtain the steady-state values of the aerodynamic parameters.

In order to solve equations (24) to (26) for the lift, drag, and pitching moment, it was necessary to obtain the terms α_t, φ_3, φ_4, T_3, and T_4 from the measured

quantities α_{lb}, φ_1, φ_2, T_1, and T_2 by the iterative procedure discussed previously. For the present tests, however, it was necessary to limit the procedure to one iteration for two reasons. First, the adjustment in the measured angles φ_1 and φ_2 had to be kept within what was believed to be a reasonable experimental error (3^o). Second, although the procedure converged for small angles of attack, it did not appear to do so at larger angles.

There was appreciable scatter in the data for repeated tests at a given angle of attack and velocity. Part of this scatter, as mentioned in reference 5, was due to small variations of ambient wind, limited length of the test runway, and oscillations in the traces on the strip-chart records. A large portion of the scatter was also due to changes in buoyancy caused by variations in the ambient temperature of the atmosphere. These variations led to uncertainties in the exact magnitude of the buoyancy force during many of the tests. To help overcome this problem, the aerodynamic forces and pitching moment (L, D, and M_Y) were plotted against dynamic pressure $\rho V^2/2$ at each angle of attack, and least-squares straight lines were fitted to the resulting data points. The aerodynamic coefficients for each angle were then derived by taking the slopes of these straight lines. The use of this method eliminated the need for the absolute value of the buoyancy force for every test and, hence, reduced the scatter in the aerodynamic coefficients from that given in reference 5. There were not enough test data to use this method for angles of attack above 16^o or for tests in which the tail fins were removed; thus, no data are presented for these cases.

The lift, drag, and pitching-moment coefficients C_L, C_D, and C_m for the 7.64-meter balloon are shown in figure 15. The curves shown are least-squares fits to the data and are given by

$$C_L = 0.82(\alpha_t - 0.023) - 5.023(\alpha_t - 0.023)^3 + 111.4(\alpha_t - 0.023)^5$$

$$C_D = 0.0487 + 186.2(\alpha_t - 0.023)^6$$

$$C_m = -0.0106 - 0.1435\alpha_t$$

where α_t is the angle of attack in radians. The particular degree of the polynomials chosen for each of these equations is a matter of judgment; however, the lift should be an odd function and the drag an even function of angle of attack, as given. In the present case, the curves are weighted so that the data points close to $\alpha_t = 0$ have the most influence on the shape of the curves. Note that the angle of zero lift (and minimum drag) is taken to be $\alpha_t = 0.023$ radian (1.3^o).

The shapes of the lift, drag, and pitching-moment curves (fig. 15) are somewhat different than expected for a normal C-class balloon. (See, e.g., refs. 16 and 17.) For the C-class balloon, the lift curve is generally more linear and the slope is steeper at lower angles of attack. Also, the drag curve generally starts to increase at lower angles of attack. These differences in the shapes of the curves are believed to be due primarily to detailed differences in the shapes of the C-class and present balloon configurations, particularly in the tail-fin assembly. The C-class tail-fin assembly generally consists of three thick fins which are not in the form of a delta wing (refs. 16 and 17), whereas the present configuration has four thin delta-wing fins. The lift-curve slope for the present case does increase with increasing angle of attack, which is consistent with the lift data for delta wings of low aspect ratio (ref. 23).

Some of the differences in the shapes of the lift, drag, and pitching-moment curves for the C-class balloon and the present balloon are also believed to be caused by deformations of the nose and tail fins of the present balloon. In an extreme case (e.g., $V = 15$ m/sec and $\alpha_t = 23^\circ$), the horizontal tail fins deformed to the extent that they failed structurally.

From the results of this investigation, it would appear that the present tow-cable technique is adequate for obtaining the lift, drag, and pitching moment for inflatable balloons. This technique is particularly useful when deformations of the balloon structure or shape are expected. If the balloon structural deformations are not important, then wind-tunnel tests with rigid models may have some advantage over the present towing technique. For rigid models, the data are not contaminated by buoyancy changes and the static lateral aerodynamic forces and moments can also be measured.

Dynamic Stability Derivatives

The results of the calculations of the dynamic stability derivatives for each planform shown in figure 11 are given in table IV. These results are based on reference values of $\bar{c}$ and S for the complete balloon and include only the tail-fin contributions to the derivatives.

As previously noted, the calculated stability derivatives for planform A are believed to be the most realistic of those presented in table IV. There are three reasons for this conclusion:

(1) The calculated value of $(C_{L_\alpha})_T$ for planform A is nearer the measured value of C_{L_α} for the complete balloon. Note that the calculated value of $(C_{L_\alpha})_T$ for each of the rigid tail-fin planforms presented in table IV is higher than the measured value for

the complete balloon $\left(\text{measured } C_{L_\alpha}\big|_{\alpha_{t=0}} = 0.82\right)$. This condition could possibly result from aeroelastic deformations of the balloon.

(2) The calculated value of $(C_{m_\alpha})_T$ for planform A is nearer the measured increment of C_{m_α} due to the tail fins. Although the experimental data measured with the tail fins on and off the hull are inadequate for a quantitative definition of tail-fin effectiveness, there were enough tail-off data to get a qualitative estimate of the tail-fin contributions to the measured value of C_{m_α}.

(3) Photographs of tufts on the lower surfaces of the horizontal tail fins indicate that except near the tips, the flow is nearly parallel to the conical aft portion of the body, as assumed for planform A.

The values of C_{m_q} estimated by calculations are quite close for all three planform treatments (table IV). Larger differences due to planform treatment are apparent in the $\dot{\alpha}$ derivatives, which generally arise from downwash-lag effects. The principal source for downwash-lag effects for conventional airplanes is the lag of downwash from the wing impinging on the tail (e.g., ref. 22). For the balloon configuration treated herein, interactions between the body and tail fins might be a similar source of downwash-lag effects, but these interactions could not be determined for the present case. Thus, these interactions are omitted here and the calculated values of $C_{L_{\dot{\alpha}}}$ and $C_{m_{\dot{\alpha}}}$ take into account only the effects of the fin on itself. The calculated value of $C_{m_{\dot{\alpha}}}$ may be underestimated as a result of the omission of body-fin interaction effects. The values of C_{L_q} and C_{l_p} for planform A are quite different from those for planforms B and C. These differences are due to differences in planform areas and locations of the aerodynamic center.

It should be noted that the linearized lifting-surface theory used to calculate the aerodynamic derivatives treats only the conditions for small angles of attack and does not include such effects as leading-edge vortex formation on highly swept planforms at angle of attack (e.g., refs. 23 and 24).

CONCLUDING REMARKS

Analytical and experimental methods have been presented for determining the stability parameters for an inflatable balloon. These methods were applied to a 7.64-meter-long balloon, and the results were presented.

Three types of stability parameters were considered in the present study. These were aerostatic properties, masses and moments of inertia, and aerodynamic coefficients

and derivatives. (The tether-cable derivatives were not included in this study but are presented in NASA TN D-7272.)

The masses and moments of inertia for the 7.64-meter balloon were determined from both analytical and experimental methods and the results of the two methods were compared. Most of the analytical results were consistent with those obtained experimentally. There were significant differences, however, between the measured and calculated values of apparent-mass inertias. These differences were attributed in some cases to the use of inadequate empirical estimates in the analytical calculations and in other cases to scatter in the experimental data.

The results of the present study indicate that the static aerodynamic lift, drag, and pitching-moment coefficients for inflated balloons can be satisfactorily measured with a double-cable towing technique. This procedure is useful when there is difficulty in simulating elastic deformations of the balloon in a wind tunnel.

The values of the aerodynamic stability derivatives calculated in this report may be somewhat crude, but they are believed to be of sufficient accuracy to warrant use in a tethered-balloon stability analysis.

Langley Research Center,
National Aeronautics and Space Administration,
Hampton, Va., April 25, 1973.

APPENDIX

EQUATIONS OF MOTION FOR THE BIFILAR PENDULUM

The equations of motion for the bifilar-pendulum system (fig. 8) are derived by summing forces in the y-direction and moments about the Z"-axis (i.e., yawing moments). If the motions in the y- and ψ-directions are small and the damping is negligible, then the equations of motion about the balloon center of mass are

$$\sum F_Y = m_{y,t}\ddot{y} + \frac{T_1 y_1}{l_1} + \frac{T_2 y_2}{l_1} = 0 \tag{A1}$$

$$\sum M_Z = I_{zz}\ddot{\psi} + \frac{T_1 c_1}{l_1} y_1 + \frac{T_2 c_2}{l_1} y_2 = 0 \tag{A2}$$

The point labeled "e.a." in figure 8 is at the intersection of the balloon center line and the elastic axis. The elastic axis is defined as the locus of points at which a lateral force can be applied and the balloon will translate laterally but will not rotate. Hence, about the elastic axis the following relationship applies:

$$T_2 l_R = T_1 l_F \tag{A3}$$

If the origin of the coordinate system is transferred to the point "e.a.," then the following relationships apply (fig. 8(b)):

$$y_1 = y_3 + l_F\psi$$

$$y_2 = y_3 - l_R\psi$$

$$y = y_3 - e_1\psi$$

$$c_1 = e_1 + l_F$$

$$c_2 = e_1 - l_R$$

$$e_1 = l_x - l_e$$

and the equations of motion (A1) and (A2) become

$$m_{y,t}\ddot{y}_3 + k_{yy}y_3 - m_{y,t}(l_x - l_e)\ddot{\psi} = 0 \tag{A4}$$

$$I_{zz}\ddot{\psi} + k_{\psi\psi}\psi + k_{yy}(l_x - l_e)y_3 = 0 \tag{A5}$$

where

$$k_{yy} = \frac{T_1 + T_2}{l_1} \tag{A6}$$

$$k_{\psi\psi} = \frac{T_1 l_F^2 + T_2 l_R^2}{l_1} \tag{A7}$$

The expression for the location of the vertical axis which has no side translation (i.e., node line) is as follows (fig. 8(b)):

$$x_n = \frac{y_3}{\psi}$$

Substituting this relationship into the equations of motion (A4) and (A5) gives

$$m_{y,t}\left(1 - \frac{l_x - l_e}{x_n}\right)\ddot{\psi} + k_{yy}\psi = 0 \tag{A8}$$

$$I_{zz}\ddot{\psi} + \left[k_{\psi\psi} + k_{yy}(l_x - l_e)x_n\right]\psi = 0 \tag{A9}$$

Since the damping is assumed negligible, the solution to equations (A8) and (A9) is in the form of

$$\psi = \psi_o e^{i\omega t}$$

where ψ_o is a constant. Substituting this relationship into equations (A8) and (A9) gives

$$m_{y,t}\left(1 - \frac{l_x - l_e}{x_n}\right) = \frac{k_{yy}}{\omega^2} \tag{A10}$$

$$I_{zz} - (l_x - l_e)x_n \frac{k_{yy}}{\omega^2} = \frac{k_{\psi\psi}}{\omega^2} \tag{A11}$$

The system analyzed has two degrees of freedom and therefore will have two possible modes. Each mode will have its own unique frequency ω and corresponding node-line location x_n. In most cases, however, the system can be excited so that one mode will dominate the motion. Thus for this condition, the system may be considered to exhibit only one mode of motion.

The terms l_e, k_{yy}, and $k_{\psi\psi}$ in equations (A10) and (A11) can be calculated from equations (A3), (A6), (A7), and the relationships (see fig. 8(a))

$$l_R + l_F = l_{TH}$$

$$l_e = l_{FC} + l_F$$

The frequency ω and the location of the node line x_n can be determined directly from the bifilar-pendulum test. Thus, the remaining unknowns in equations (A10) and (A11) are I_{zz}, $m_{y,t}$, and l_x.

REFERENCES

1. Bairstow, L.; Relf, E. F.; and Jones, R.: The Stability of Kite Balloons: Mathematical Investigation. R. & M. No. 208, Brit. A.R.C., 1915.

2. Neumark, S.: Equilibrium Configurations of Flying Cables of Captive Balloons, and Cable Derivatives for Stability Calculations. R. & M. No. 3333, British A.R.C., 1963.

3. DeLaurier, James D.: A Stability Analysis of Cable-Body Systems Totally Immersed in a Fluid Stream. NASA CR-2021, 1972.

4. DeLaurier, James D.: A First Order Theory for Predicting the Stability of Cable Towed and Tethered Bodies Where the Cable Has a General Curvature and Tension Variation. VKI-TN-68, Von Karman Inst. Fluid Dyn., Dec. 1970.

5. Redd, L. Tracy: A Towing Technique for Determining the Aerodynamic Forces on Tethered Balloons. Paper presented at Sixth Air Force Cambridge Research Laboratories Scientific Balloon Symposium (Portsmouth, N.H.), June 1970.

6. Redd, L. Tracy; Bland, Samuel R.; and Bennett, Robert M.: Stability Analysis and Trend Study of a Balloon Tethered in a Wind, With Experimental Comparisons. NASA TN-7272, 1973.

7. Bennett, Robert M.; Bland, Samuel R.; and Redd, L. Tracy: Computer Programs for Calculating and Plotting the Stability Characteristics of a Balloon Tethered in a Wind. NASA TM X-2740, 1973.

8. Redd, L. Tracy; Bennett, Robert M.; and Bland, Samuel R.: Analytical and Experimental Investigation of the Stability of a Balloon Tethered in a Wind. Paper presented at Seventh Air Force Cambridge Laboratories Scientific Balloon Symposium (Portsmouth, N.H.), Sept. 1972.

9. DeLaurier, James D.: A Stability Analysis for Tethered Aerodynamically Shaped Balloons. J. Aircraft, vol. 9, no. 9, Sept. 1972, pp. 646-651.

10. Vorachek, Jerome J.; Burbick, James W.; and Doyle, George R., Jr.: Investigation of Dynamic Behavior of Tethered Balloon Systems. AFCRL-72-0113, U.S. Air Force, 1972.

11. Zahm, A. F.; Smith, R. H.; and Louden, F. A.: Drag of C-Class Airship Hulls of Various Fineness Ratios. NACA Rep. 291, 1928.

12. Anon.: Standard Atmosphere – Tables and Data for Altitudes to 65,800 Feet. NACA Rep. 1235, 1955. (Supersedes NACA TN 3182.)

13. Landweber, L.; and Winzer, A.: A Comparison of the Added Masses of Streamlined Bodies and Prolate Spheroids. Rep. 572 (Contract N6-onr-24 705), Exp. Towing Tank, Stevens Inst. Technol., June 1955.

14. Malvestuto, Frank S., Jr.; and Gale, Lawrence J.: Formulas for Additional Mass Corrections to the Moments of Inertia of Airplanes. NACA TN 1187, 1947.

15. Dunning, Robert S.: Experimental Determination of Apparent Mass and Moment of Inertia of a Large Disk Suspended as a Pendulum at Different Air Densities. NASA TN D-5897, 1970.

16. Stein, Donald E.; and Shindo, Shajiro: A Wind Tunnel Test of a Single Hulled Balloon at Extreme Angle of Attack. Rep. 901, Aeronaut. Lab., Univ. of Washington, Feb. 27, 1968.

17. Farmer, James R.; and Shindo, Shajiro: A Wind Tunnel Test of Three Single Hulled Balloons and One Double Hulled Balloon at Extreme Angles of Attack. Rep. 957 B, Aeronaut. Lab., Univ. of Washington, [1969].

18. Robinson, M. L.: The Estimation of Pitch Damping Derivatives of Missile Configurations at Subsonic Speeds. AIAA Paper No. 70-537, May 1970.

19. Miles, John W.: The Potential Theory of Unsteady Supersonic Flow. Cambridge Univ. Press, 1959.

20. Rodden, William P.; and Giesing, Joseph P.: Application of Oscillatory Aerodynamic Theory to Estimation of Dynamic Stability Derivatives. J. Aircraft, vol. 7, no. 3, May-June 1970, pp. 272-275.

21. Watkins, Charles E.; Woolston, Donald S.; and Cunningham, Herbert J.: A Systematic Kernel Function Procedure for Determining Aerodynamic Forces on Oscillating or Steady Finite Wings at Subsonic Speeds. NASA TR R-48, 1959.

22. Etkin, Bernard: Dynamics of Flight. John Wiley & Sons, Inc., c.1959.

23. Polhamus, Edward C.: A Concept of the Vortex Lift of Sharp-Edge Delta Wings Based on a Leading-Edge-Suction Analogy. NASA TN D-3767, 1966.

24. Boyden, Richmond P.: Effects of Leading-Edge Vortex Flow on the Roll Damping of Slender Wings. J. Aircraft, vol. 8, no. 7, July 1971, pp. 543-547.

TABLE I.- HULL DIMENSIONS FOR THE 7.64-METER BALLOON

Station	Distance along balloon axis of symmetry from nose, m	Radius, m
0	0	0
1	.05	.25
2	.10	.38
3	.20	.60
4	.41	.88
5	.61	1.06
6	.81	1.15
7	1.02	1.21
8	1.22	1.24
9	1.42	1.27
10	1.63	1.27
11	1.83	1.27
12	2.03	1.26
13	2.24	1.24
14	2.44	1.22
15	2.64	1.19
16	2.84	1.16
17	3.05	1.12
*18	3.25	1.08
19	4.88	.71
20	7.64	.10

*Point of tangency of the aft conical section with the C-class section.

TABLE II.- AEROSTATIC PROPERTIES OF THE 7.64-METER BALLOON

Buoyancy, B, N	190
Center of buoyancy, b, m	2.48
Mass of inflation gas, m_g, kg	3.22
Reference length, $\bar{c}$, m	7.64
Structural center of mass, a, m	4.72
Structural weight, W_S, N	84.2
Volume, V_b, m^3	19.0

TABLE III.- ANALYTICAL AND EXPERIMENTAL VALUES OF MASS AND INERTIA FOR THE 7.64-METER BALLOON

Parameter	Analytical	Experimental	Best estimate
Structure			
a, m	4.51	4.72	4.72
m_s, kg	8.28	8.58	8.58
$I_{xx,s}$, kg-m^2	6.64	6.81	6.81
$I_{yy,s} = I_{zz,s}$, kg-m^2	56.5	54	56.5
Inflation gas			
b, m	2.65	2.58	2.58
m_g, kg	3.08	3.22	3.22
$I_{xx,g}$, kg-m^2	1.83	0.24	0.24
$I_{yy,g} = I_{zz,g}$, kg-m^2	7.90	----	7.90
Apparent mass			
c, m	3.56	2.79	3.56
$m_{x,a}$, kg	5.11	5.11	5.11
$m_{y,a} = m_{z,a}$, kg	23.9	23.0	23.9
$I_{xx,a}$, kg-m^2	2.78	1.58	1.58
$I_{yy,a} = I_{zz,a}$, kg-m^2	76.5	19	76.5
Total balloon*			
l_x, m	3.70	3.25	3.70
$m_{x,t}$, kg	14.3	16.9	16.9
$m_{y,t} = m_{z,t}$, kg	35.3	34.8	35.7
I_{xx}, kg-m^2	11.2	8.63	8.63
$I_{yy} = I_{zz}$, kg-m^2	150	105	155

*The magnitudes of the terms l_x, $m_{x,t}$, $m_{y,t}$, $m_{z,t}$, I_{xx}, I_{yy}, and I_{zz} are different in reference 6 because the mass of the bridle and attached test instruments is added to the mass of the hull structure.

TABLE IV.- CALCULATED TAIL-FIN CONTRIBUTIONS TO STABILITY DERIVATIVES*

Derivative	Tail-fin contributions for –		
	Planform A	Planform B	Planform C
$(C_{L_\alpha})_T$	0.952	1.19	1.21
$C_{L_{\dot{\alpha}}}$	.089	.241	.342
C_{L_q}	.685	.847	.855
$(C_{m_\alpha})_T$	-.247	-.236	-.182
$C_{m_{\dot{\alpha}}}$	-.026	-.061	-.066
C_{m_q}	-.189	-.201	-.193
C_{l_p}	-.0237	-.0156	-.0156

*Based on S and $\bar{c}$ for complete balloon; moments are about the reference point.

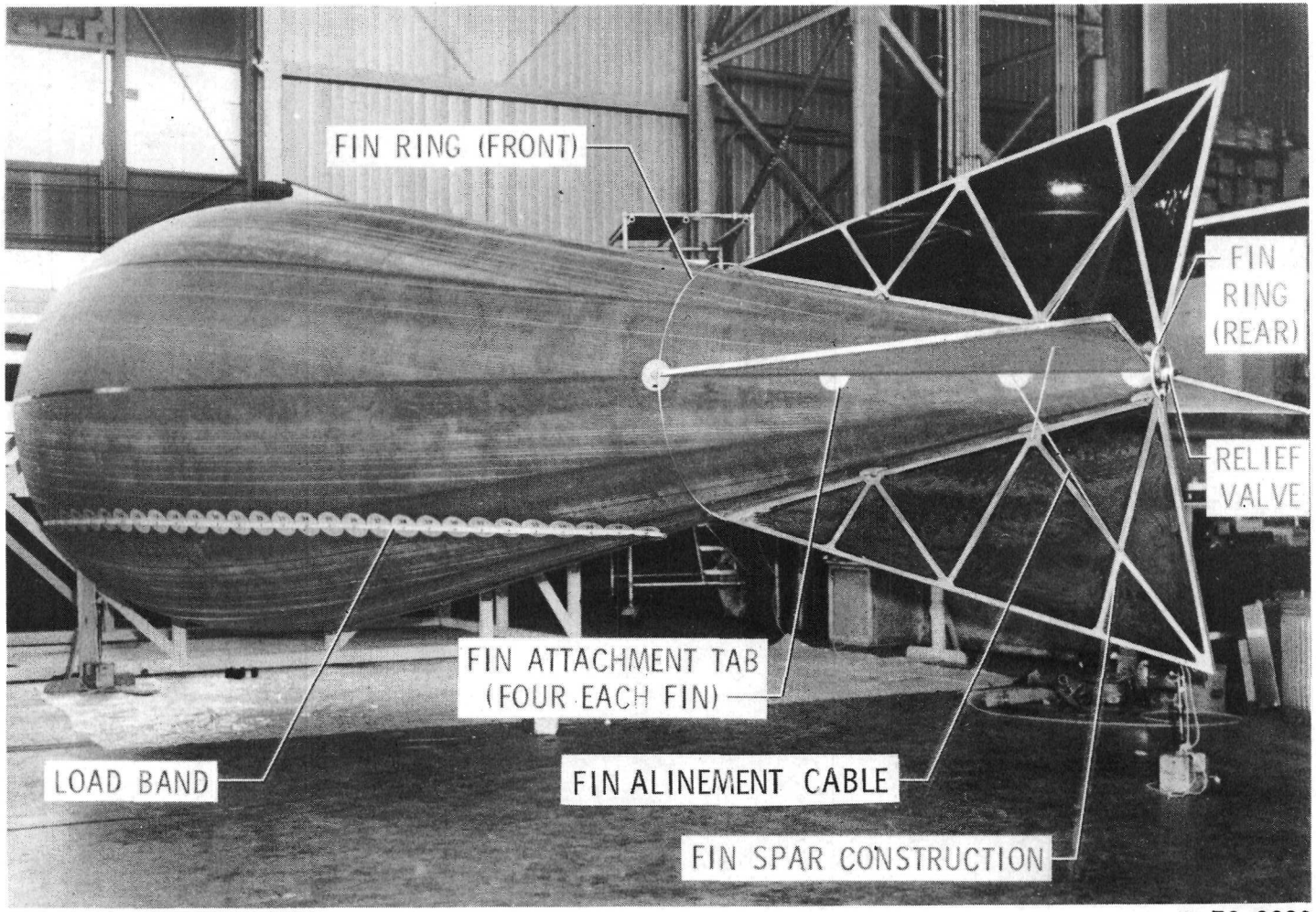

L-73-3033

Figure 1.- The 7.64-meter balloon.

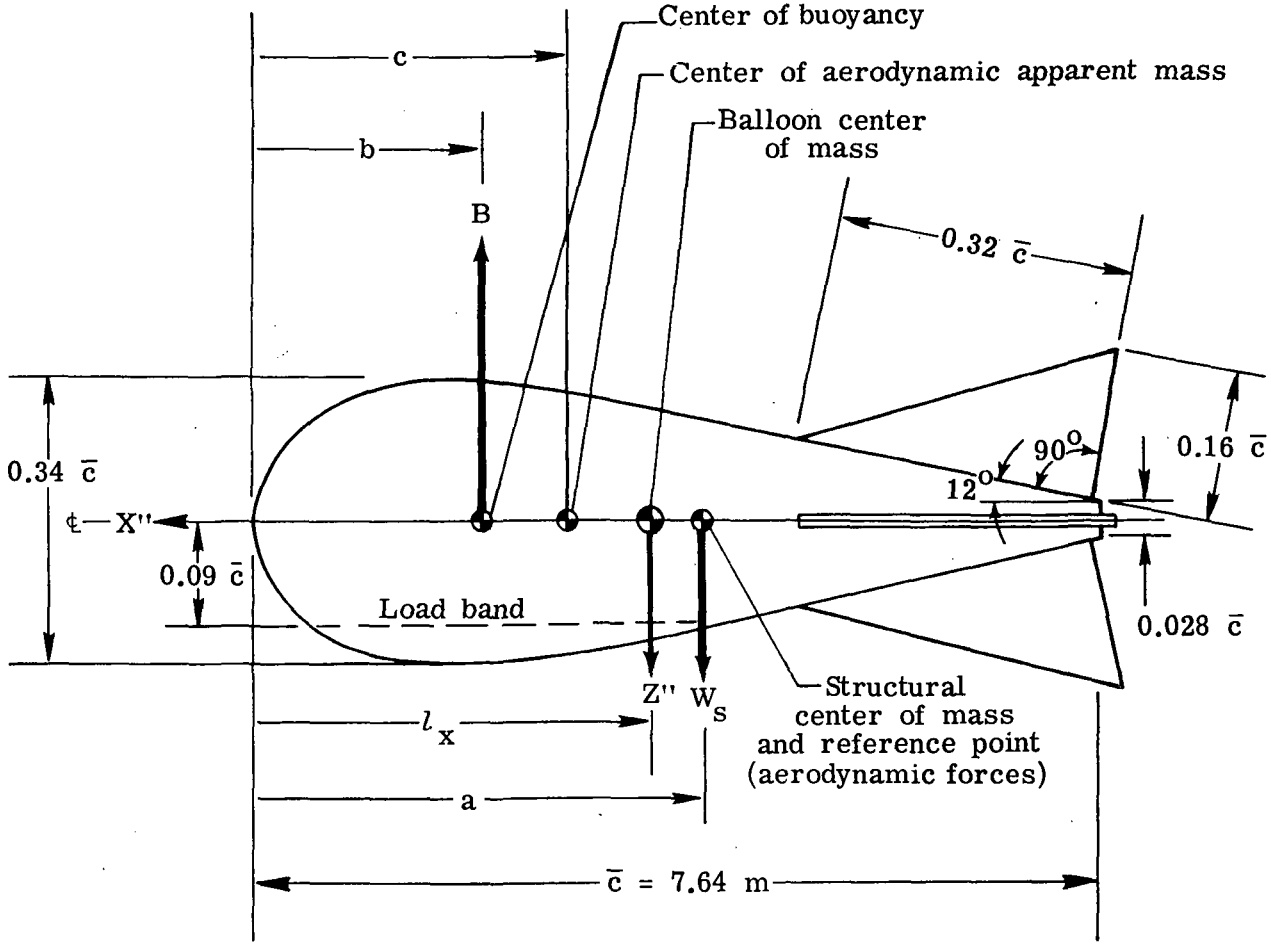

Figure 2.- Geometrical properties of the 7.64-meter balloon.

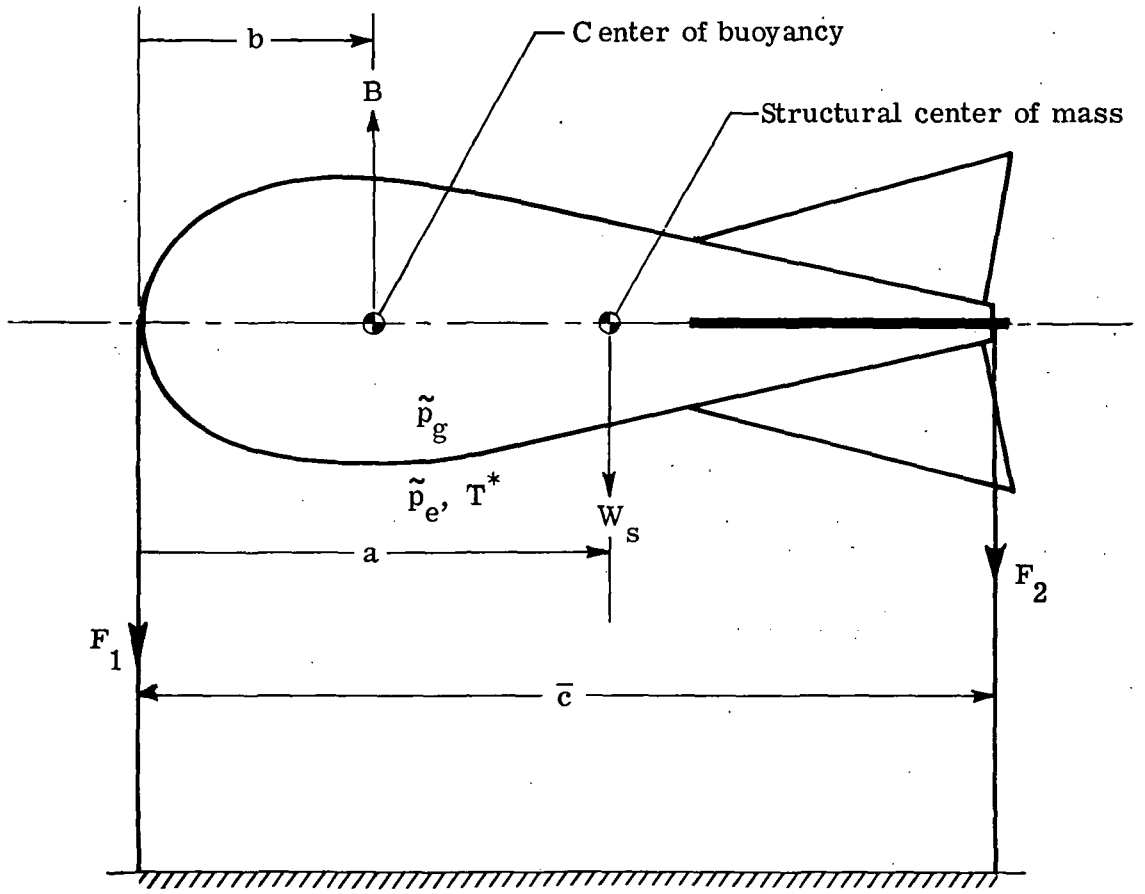

Figure 3.- Test setup to determine buoyancy force and volume of the balloon. Helium inflated.

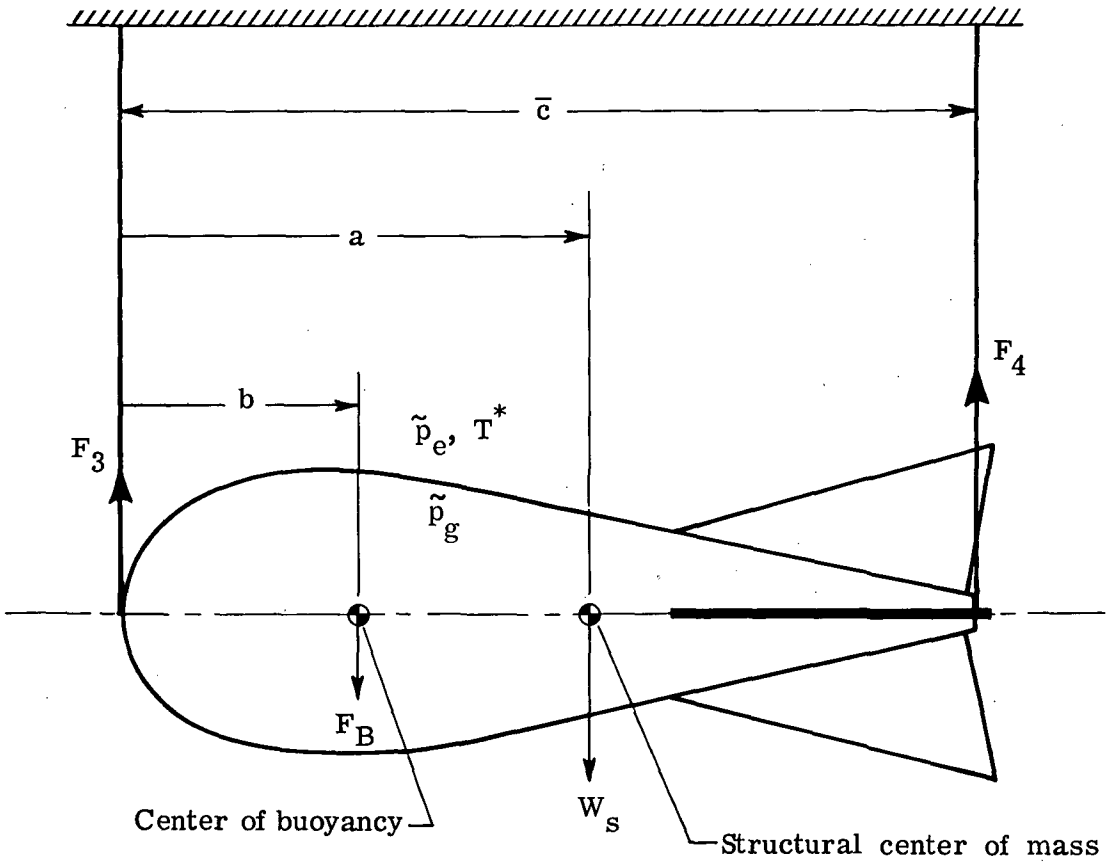

Figure 4.- Test setup to determine the structural center of mass and center of buoyancy of the balloon. Air inflated.

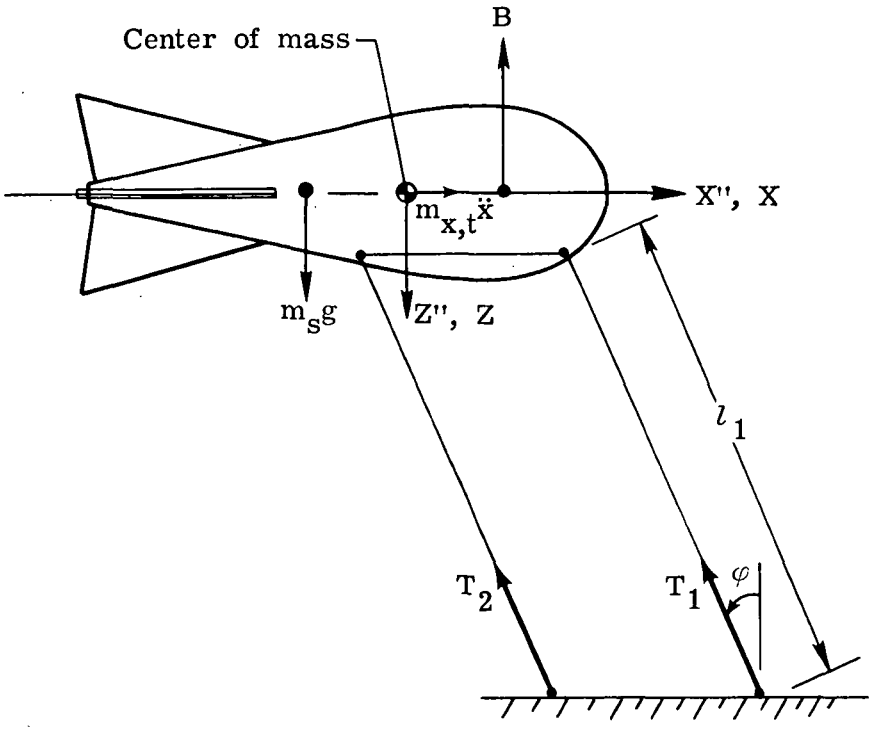

Figure 5.- Test setup to determine longitudinal apparent mass $m_{x,a}$.

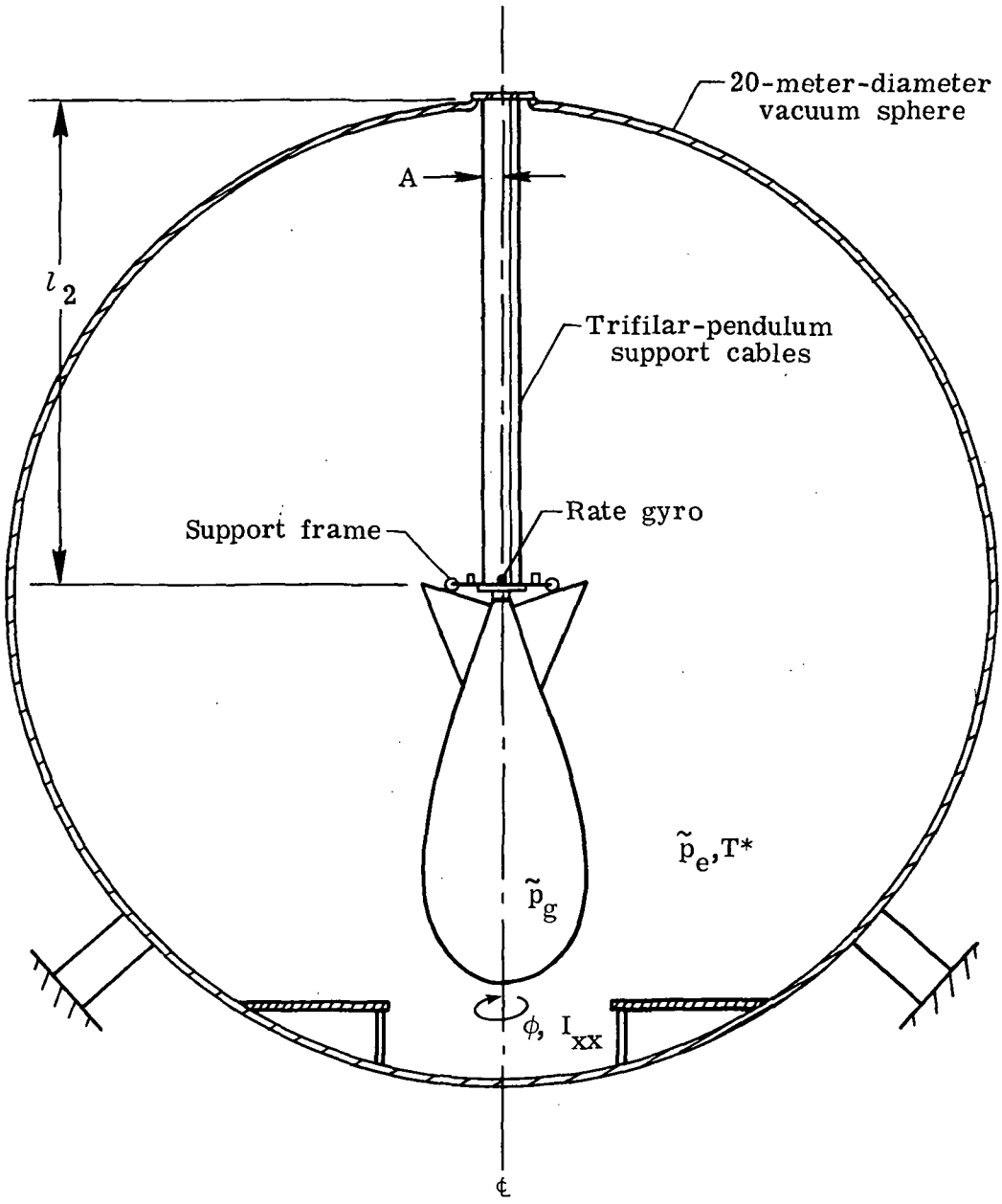

Figure 6.- Roll-inertia test setup.

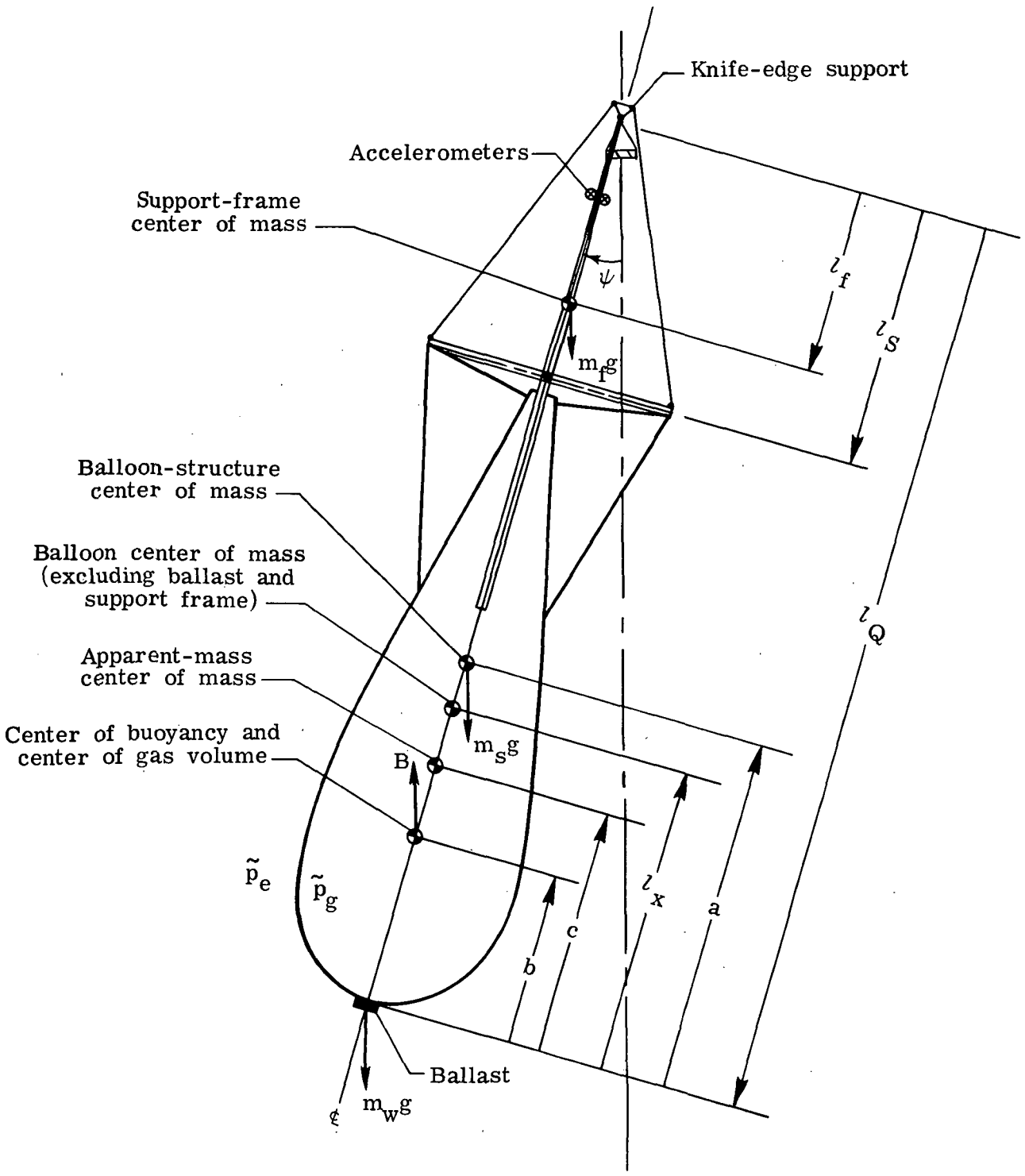

Figure 7.- Compound-pendulum test setup.

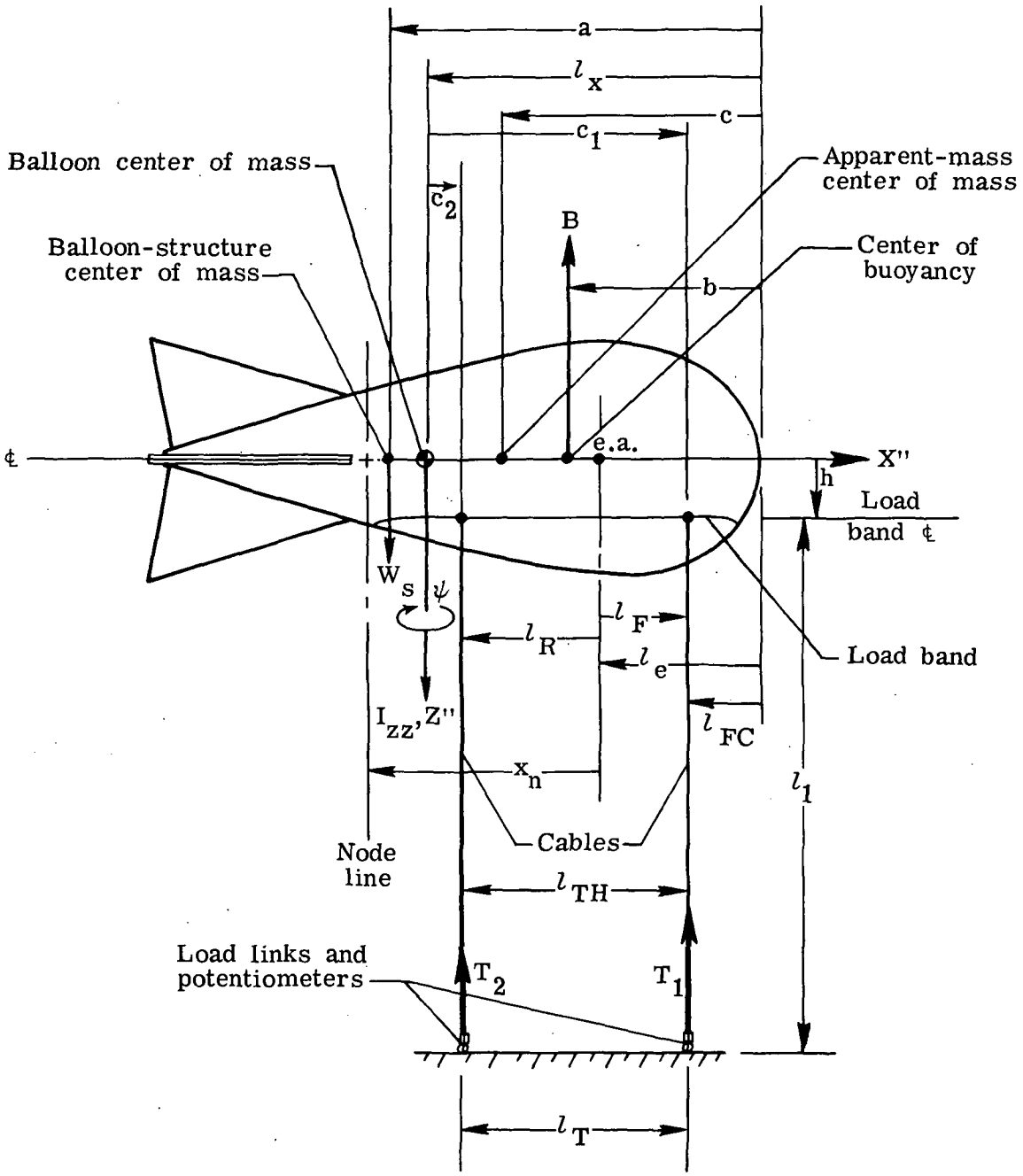

(a) Test setup.

Figure 8.- Bifilar pendulum.

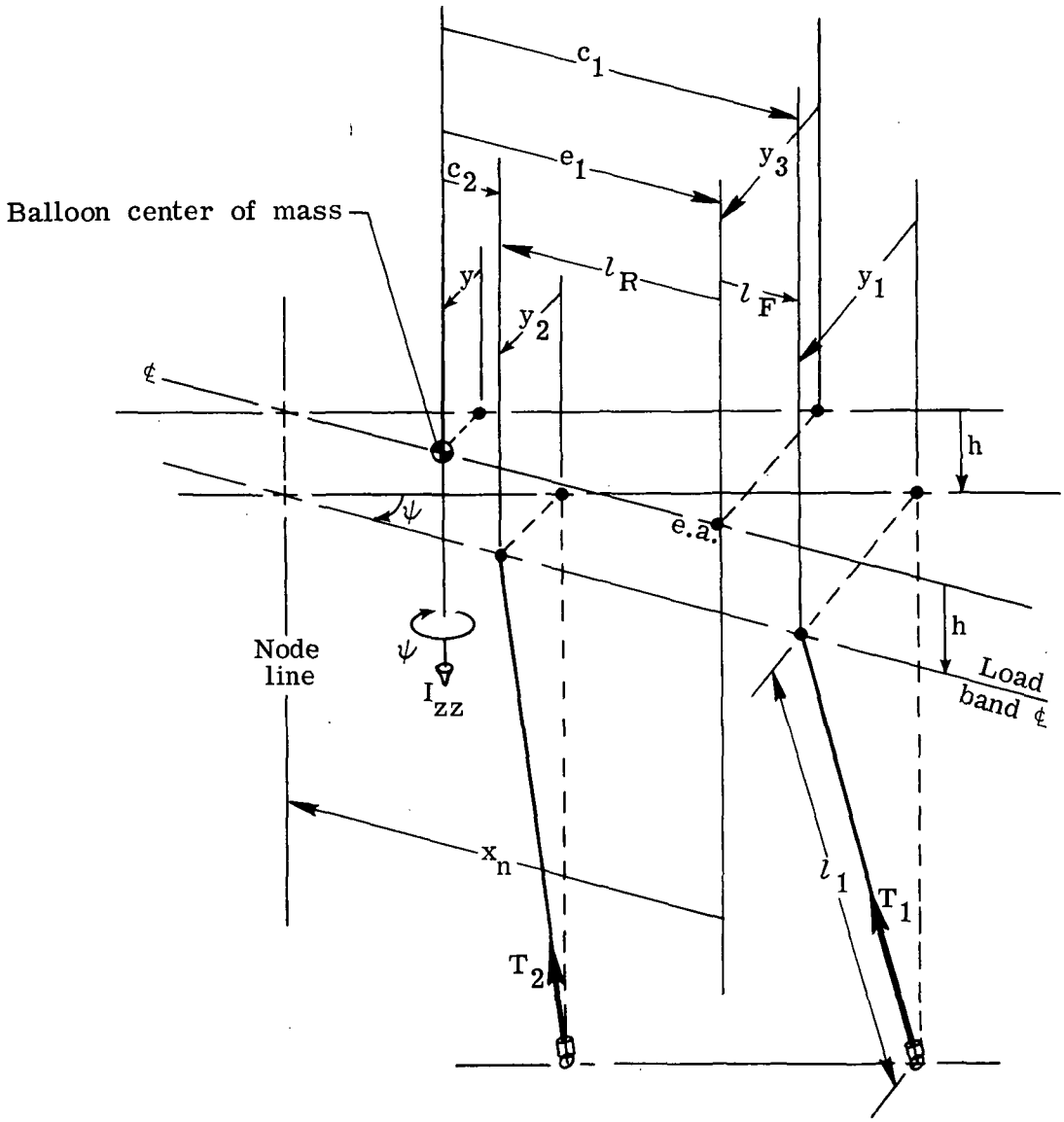

(b) Geometrical representation.

Figure 8.- Concluded.

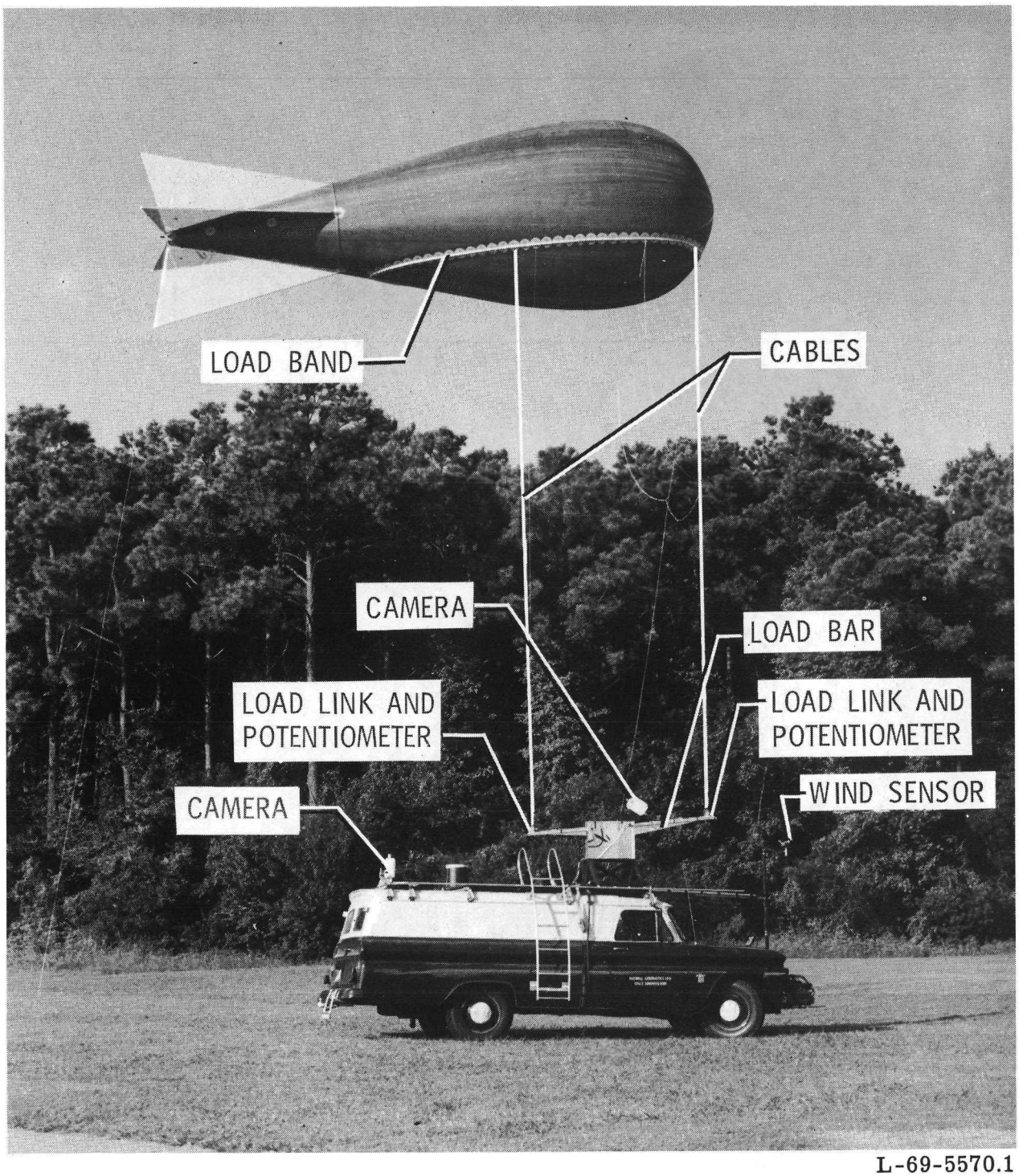

L-69-5570.1

Figure 9.- Test balloon and tow truck.

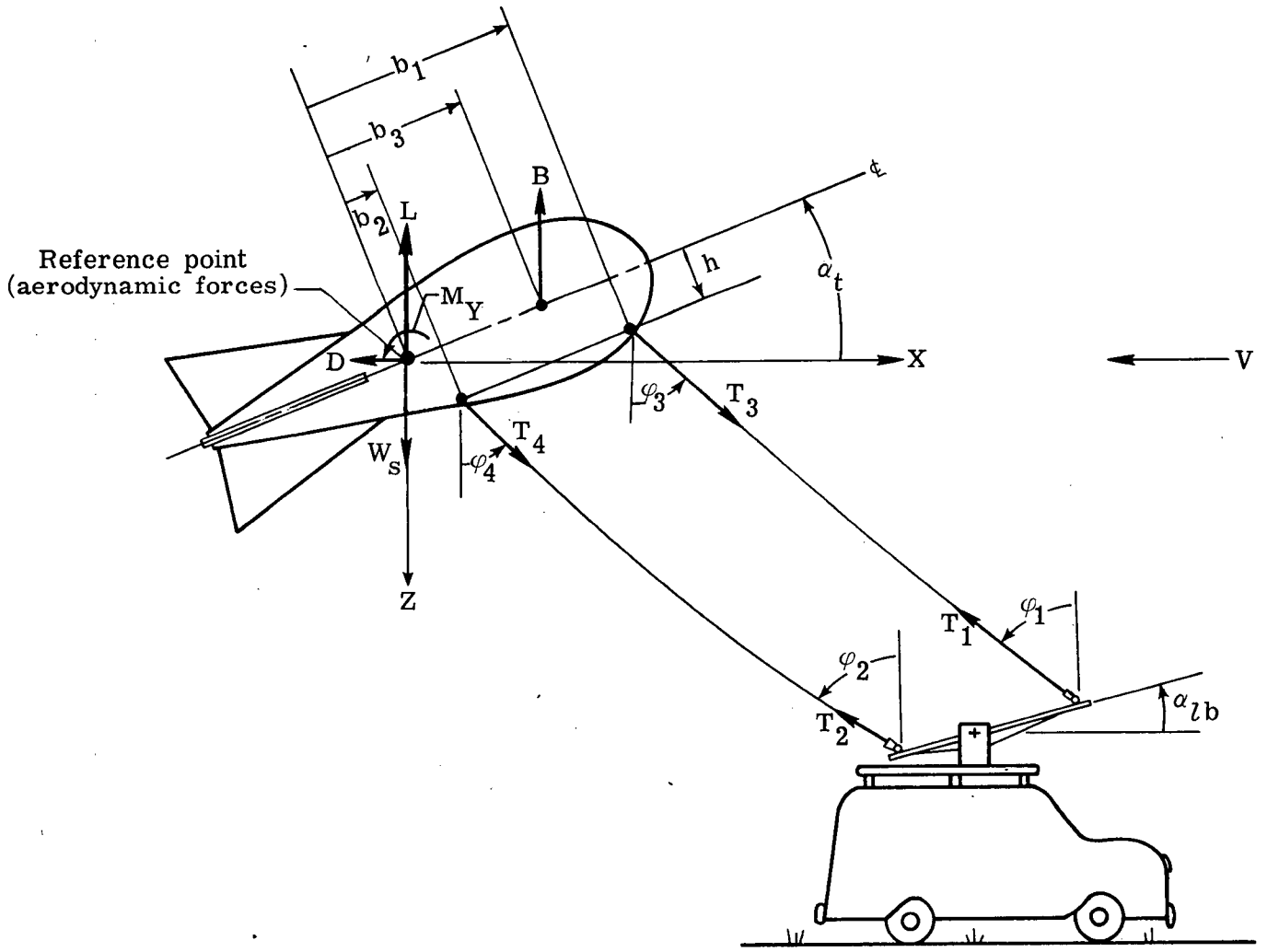

Figure 10.- Tow-test setup.

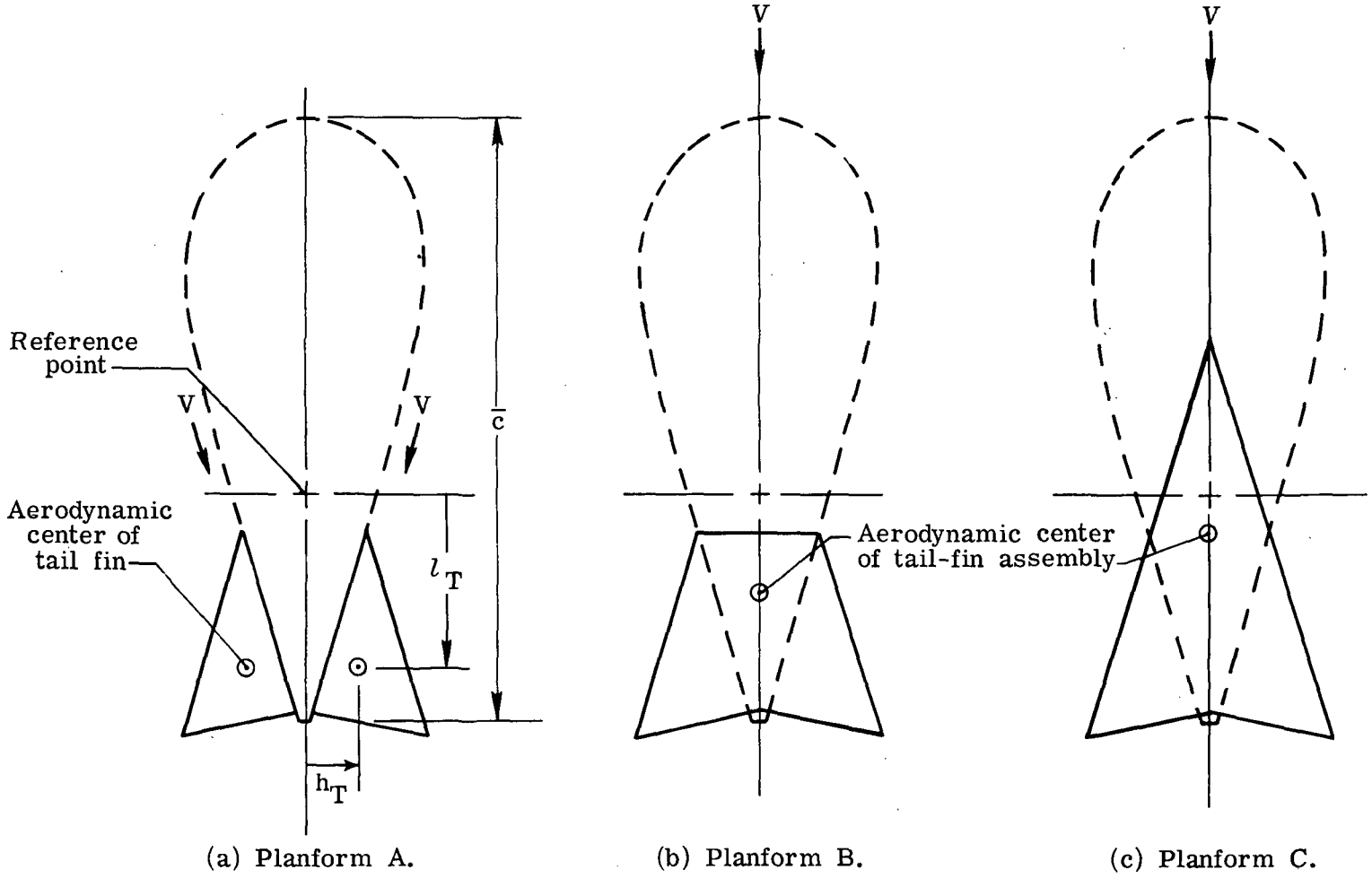

(a) Planform A. (b) Planform B. (c) Planform C.

Figure 11.- Tail-fin planforms considered for calculating tail-fin contributions to stability derivatives.

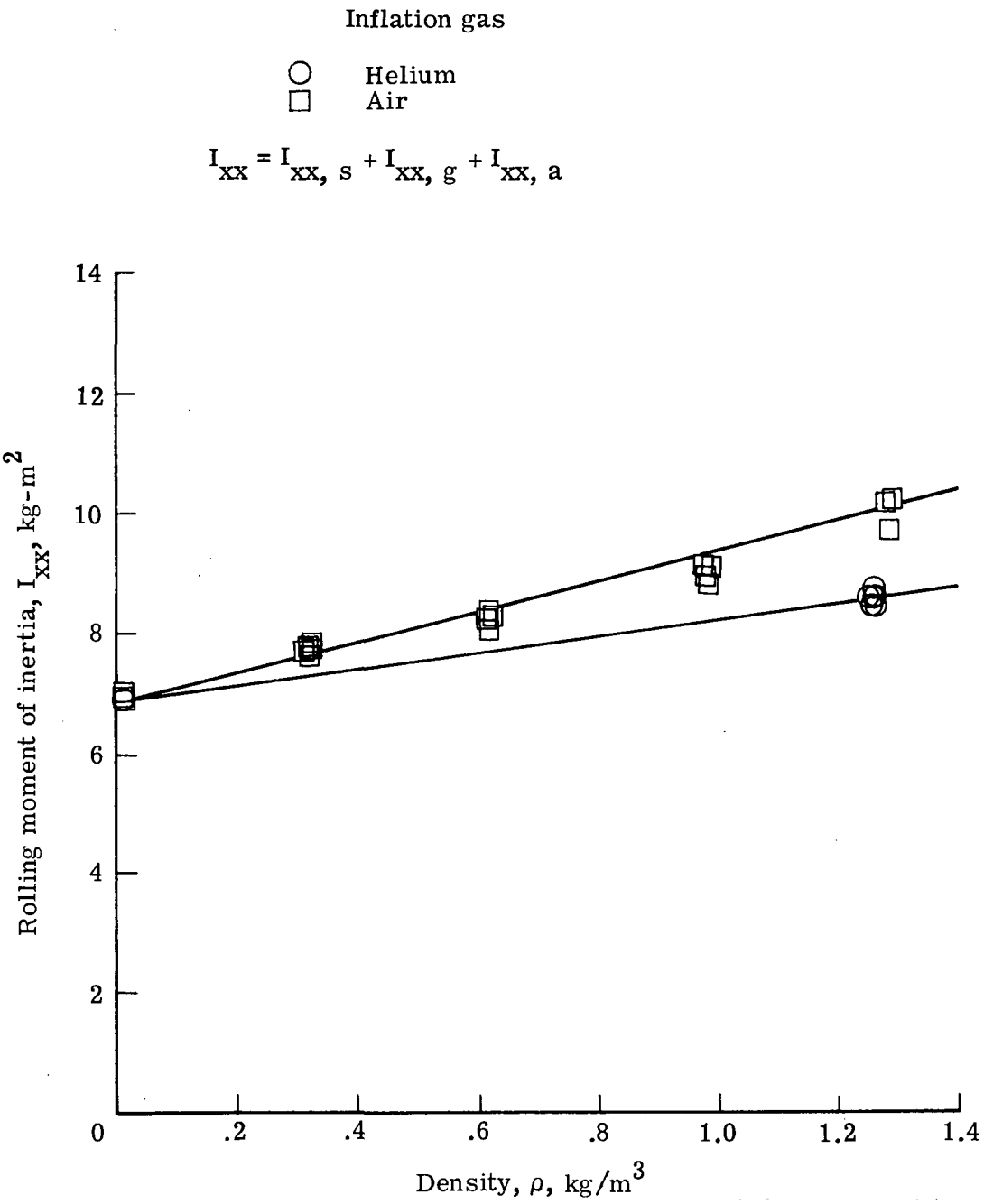

Figure 12.- Measured combined rolling moments of inertia of the balloon structure, inflation gas, and apparent mass about the axis of symmetry as a function of chamber density.

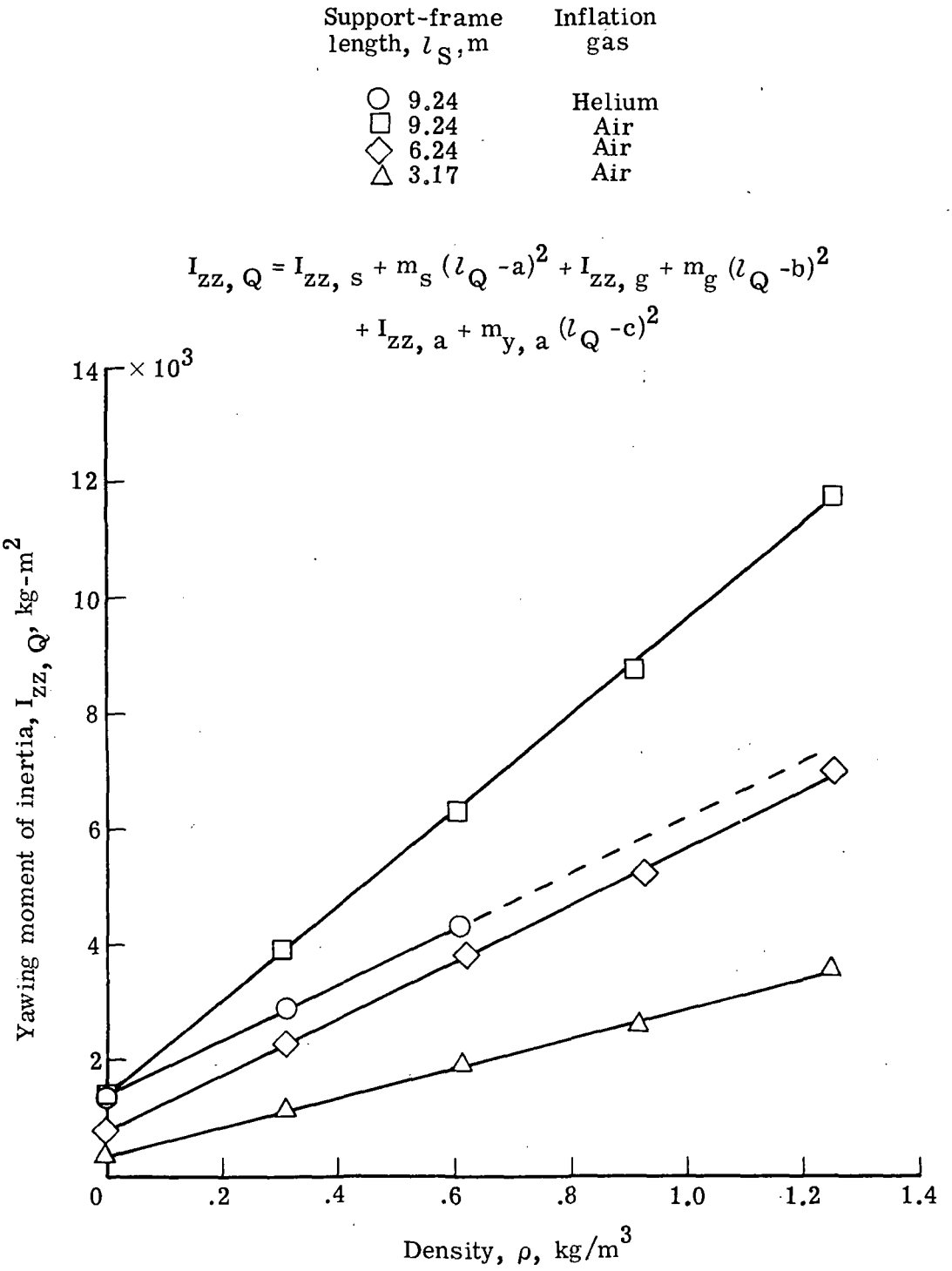

Figure 13.- Measured combined yawing moments of inertia of the balloon structure, inflation gas, and apparent mass about the knife-edge support as a function of vacuum-chamber density. (Each symbol represents the average of several test values.)

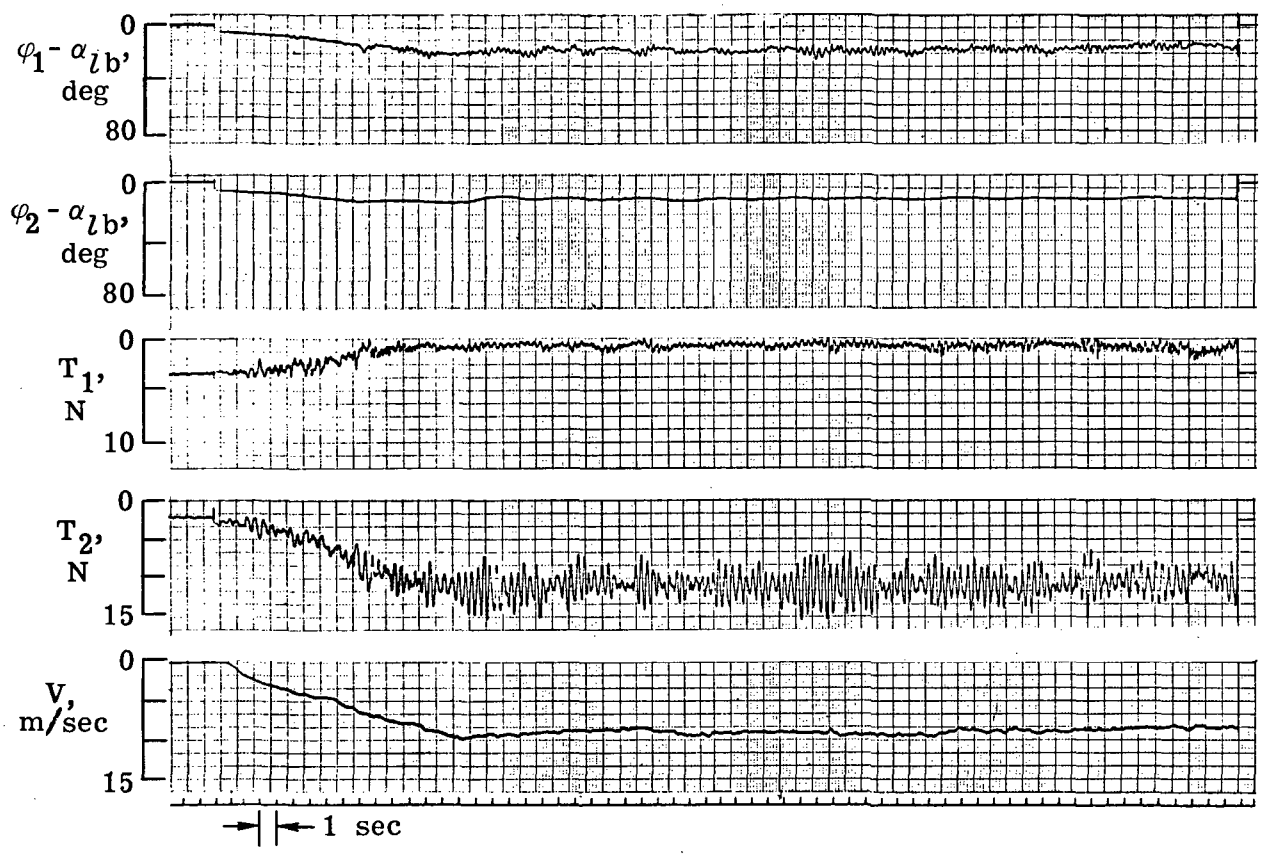

Figure 14.- Sample strip chart recording of tow-test data. $\alpha_t = 10.3^{\circ}$.

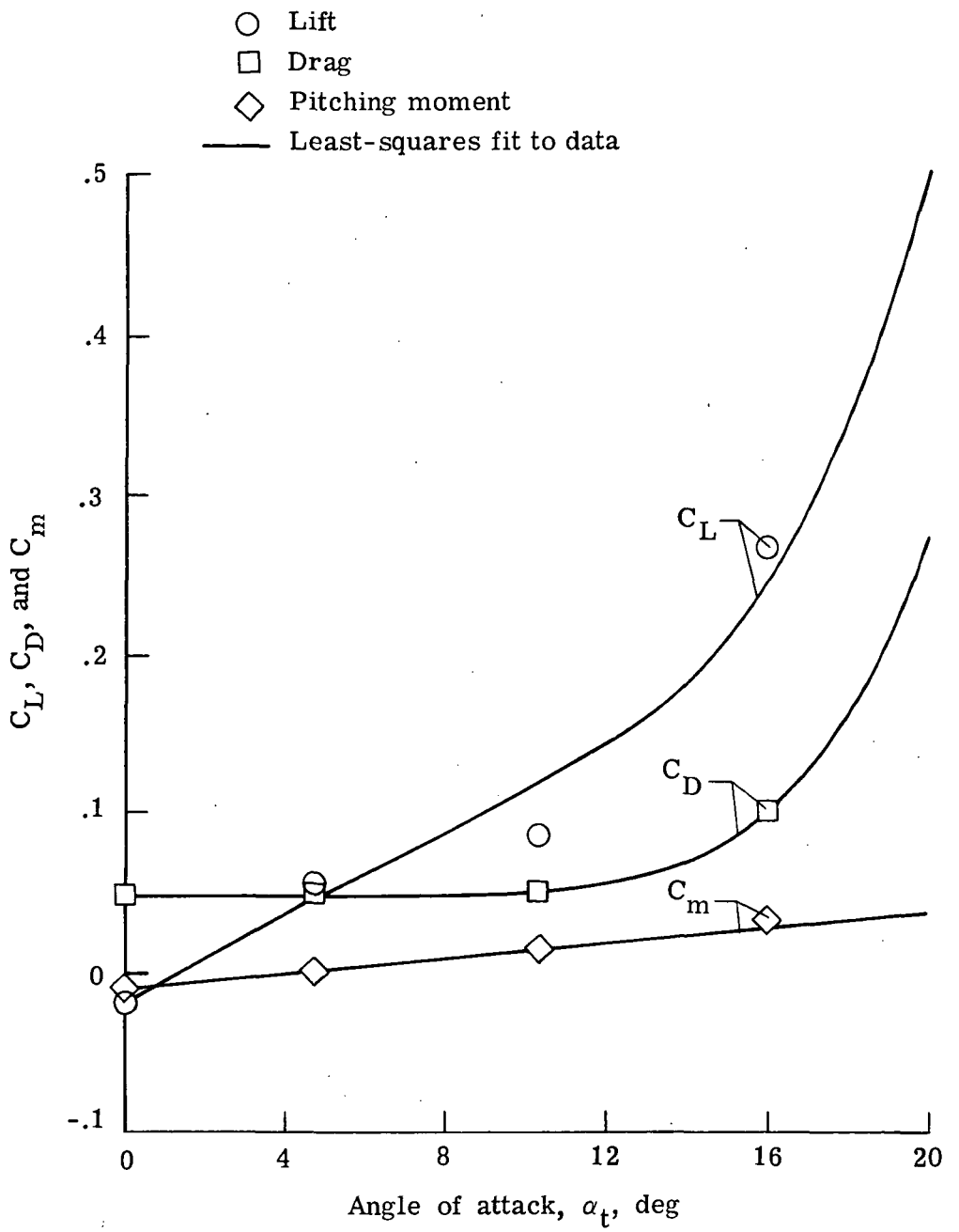

Figure 15.- Static aerodynamic coefficients as functions of angle of attack for the test balloon. (Pitching moment is about the reference point.)

NATIONAL AERONAUTICS AND SPACE ADMINISTRATION
WASHINGTON, D.C. 20546

OFFICIAL BUSINESS
PENALTY FOR PRIVATE USE $300

SPECIAL FOURTH-CLASS RATE BOOK

POSTAGE AND FEES PAID
NATIONAL AERONAUTICS AND SPACE ADMINISTRATION
451

U.S.MAIL

POSTMASTER: If Undeliverable (Section 158 Postal Manual) Do Not Return

"The aeronautical and space activities of the United States shall be conducted so as to contribute . . . to the expansion of human knowledge of phenomena in the atmosphere and space. The Administration shall provide for the widest practicable and appropriate dissemination of information concerning its activities and the results thereof."

—NATIONAL AERONAUTICS AND SPACE ACT OF 1958

NASA SCIENTIFIC AND TECHNICAL PUBLICATIONS

TECHNICAL REPORTS: Scientific and technical information considered important, complete, and a lasting contribution to existing knowledge.

TECHNICAL NOTES: Information less broad in scope but nevertheless of importance as a contribution to existing knowledge.

TECHNICAL MEMORANDUMS: Information receiving limited distribution because of preliminary data, security classification, or other reasons. Also includes conference proceedings with either limited or unlimited distribution.

CONTRACTOR REPORTS: Scientific and technical information generated under a NASA contract or grant and considered an important contribution to existing knowledge.

TECHNICAL TRANSLATIONS: Information published in a foreign language considered to merit NASA distribution in English.

SPECIAL PUBLICATIONS: Information derived from or of value to NASA activities. Publications include final reports of major projects, monographs, data compilations, handbooks, sourcebooks, and special bibliographies.

TECHNOLOGY UTILIZATION PUBLICATIONS: Information on technology used by NASA that may be of particular interest in commercial and other non-aerospace applications. Publications include Tech Briefs, Technology Utilization Reports and Technology Surveys.

Details on the availability of these publications may be obtained from:

SCIENTIFIC AND TECHNICAL INFORMATION OFFICE

NATIONAL AERONAUTICS AND SPACE ADMINISTRATION

Washington, D.C. 20546